Investigating a glacier tidewater collapse and dynamics: Negribreen in Eastern Svalbard

Odin Næss Haga

Institutt for Geofag

Faculty of mathematics and natural sciences

UNIVERSITY OF OSLO

June 1, 2019

2019

Investigating a glacier tidewater collapse and dynamics: Negribreen in Eastern Svalbard

http://www.duo.uio.no/

Printed: Reprosentralen, University of Oslo

Abstract

Negribreen, a tidewater glacier located in mid-eastern Svalbard, experienced a collapsed after summer 2016. This resulted in ice horizontal velocities above 22 meters per day making it one of the fastest flowing glaciers on the archipelago. The last surge is thought to have occurred in the 1930s, but due to a very long quiescent phase, prior investigations of this glacier have been limited. As Negribreen is part of one of the largest glacier systems in Svalbard, investigating its current surge event will provide important information on surge behavior within the region. Here, we demonstrate the surge development and triggering mechanisms using a time series of digital elevation models, velocities and glacier extents from various sources. The analysis show that the triggering mechanisms are subdivided within two phases. (1) A long-lasting phase with a slow flow regime, changing the glacier's geometry over decades. Eventually, this lowers the friction at the bed by introducing basal melt and initiates surface deformation, which signals the changeover to phase (2). In this phase the glacier advances and experience a rapid velocity growth and surface lowering which further lubricates the bed through an evolving up-propagating crevasse field. This phase is short-lived and shear stresses quickly overcome an internal threshold which triggers the collapse. The observed behaviors in both phases show strong similarities to other surging glaciers on Svalbard and suggests a general outline for surge behavior on tidewater glaciers in the region.

Acknowledgement

A special gratitude I give to my supervisors Christopher Nuth and Robert McNabb, who provided me with good guidance in this thesis and interesting conversations. Thanks to Bas Altena and Thomas Schellenberger for providing velocities from Sentinel-2 and ERS 1-2. I also want to thank all other data providers, including the National Snow and Ice Data Center , Norsk Polarinstitutt, the ActicDEM project, the European Space Agency and others who dedicate a lot of time making good data products and shares them freely with the public.

Contents

List of Figures

List of Tables

1 Introduction

The cryosphere relates to the parts of Earth's systems that have been influenced of temperatures below 0° Celsius for at least a year and contains water in its frozen form (Subcommittee, 1988). It comprises snow, river and lake ice, sea ice, glaciers, ice shelves and ice sheets, and frozen ground and has been a part of Earth's environmental system at several points throughout Earth's 4.6 billion history (Eyles, 2008). Ongoing changes in the cryosphere plays an important role in the surface energy budget, the water cycle, surface gas exchange, primary productivity and sea level (Vaughan et al., 2013). Recent assessments indicate several critical changes occurring in the cryosphere (Vaughan et al., 2013). These changes include; an increase of permafrost temperatures (Jafarov et al., 2012), a decrease of spring snow cover extent (Brown et al., 2010), delays of river and lake ice and earlier ice break up (Brown and Duguay, 2011), ice mass loss from glaciers and ice caps (Rignot et al., 2008; Gardner et al., 2011), Arctic sea-ice decline (Tivy et al., 2011; Stroeve et al., 2012), and continuing retreat and collapse of ice shelves and ice mass loss on Antarctica and Greenland ice sheet (Vaughan et al., 2013). These changes are critical because they give direct feedback on the climate that causes concern for future societies and the biodiversity. This makes understanding the cryosphere important, because this can provide more reliable models for future climate predictions.

Sea-level rise is considered to be among the most potential damaging effect of climate change (Domingues et al., 2008). The International Panel on Climate Change (IPCC), has since the first Assessment Report back in 1990 made predictions of global sea level change. The trend measured by satellite altimeters since then has shown that sea level rise continues to run near the upper limited of the projected uncertainty range given in the third and fourth IPCC Assessment Reports (Rahmstorf et al., 2012). As these projections are important for preparation and decision making for many societies, gaining understanding of all dynamic processes linked to sea level changes is important.

This is why glaciers and ice sheets have been heavily investigated. Ice sheets and in particular glaciers are sensitive barometers to climate change, constantly growing and shrinking in relation to temperature, snowfall and other climatic factors. Although the

Greenland and Antarctica ice sheets store by far the most amount of water, with a sea-level equivalent of >60m compared to between 15 and 37 cm on glaciers and smaller ice caps, it is the smaller glaciers and ice caps that are excpected to be the greatest contributions to near-future sea-level rise (Dyurgerov et al., 2005). In the period of 1993-2010, mass loss from glaciers have contributed 27 % of the total to sea-level rise (Martín Español et al., 2015). This makes understanding all dynamics processes linked to glaciers important.

2 Background

2.1 Glacier dynamics

The force balance

Glacier flow is a balance between driving and resistive stresses. The driving stress is defined as:

$$\rho g_i H \tan \alpha \tag{1}$$

with density (ρ), gravity acceleration (g), ice thickness (H) and (α) the surface slope of the ice. Resistance to flow comprises of drag along the ice and bed interface (basal drag), the sides of the glacier (lateral drag) and from spatial variation in pulling or pushing forces (longitudinal stress gradients). Lateral drag arises where the bed resistance varies in the cross/flow direction. This can occur at the margins of a valley or where there are lateral changes in bed roughness, substrate type, basal temperature or water pressure (Raymond, 1996). The longitudinal stress gradient is the result of variations in along-flow directed deviatoric stresses. In combination, the forces driving and resisting ice flow define the force balance. In the x-direction, measured in the direction of flow, this can be stated as:

$$\rho g_i H \tan \alpha = \tau_b - \frac{\partial(H\overline{\tau}_{xy})}{\partial y} - \frac{\partial(H\overline{\sigma}_x)}{\partial x} \tag{2}$$

The driving stress is on the left side and is balanced by the combined terms on the right. The first of these are the basal drag (τ_b), second the lateral drag, where τ_{xy} is the shear stress acting parallel to the sides of the glacier, and lastly the longitudinal stress gradients where σ_x is the longitudinal deviatoric stress acting in the direction of flow.

Deformation of ice

In response to stress, ice will either fracture or creep. Of these two responses, creep is the most important process of glacial motion. Fracturing will not be explained in this subsection, although it includes several important processes such as iceberg calving, glacitectonic deformation and weakening of ice streams and ice shelf margins.

Creep can be explained as deformation occurring within or between individual ice crystals from movement. Within ice crystals, flow occurs by gliding along cleavage planes

or along crystal defects, whereas movement between them occur in zones with recrystallization at grain boundaries. The most widely used law to describe the relationship of ice creep and stress is Glens flow law Glen (1955). This was first adapted for glaciers by Nye (1957) and is more fully referred to as Nye's generalization of Glen's flow law:

$$\varepsilon_{xy} = A\sigma_e^{n-1}\tau_b \tag{3}$$

where τ_b is the basal shear stress, σ_e the effective stress that incorporates all the stress components. Parameter n is defined as the exponent. The parameter A is related to the ice temperature, fabric, water content, density and grain size.

Sliding

Sliding refers to slipping between the ice and bed. The temperature at this interface is a major factor determining the sliding properties of a glacier. On frozen beds, it was previously thought before that ice movement only occurred by creep. Theoretical work and field observations showed nonetheless that some movement may still occur (Fowler, 1986; Weber, 2000). Even at low temperatures, thin films of solute content can still be present. This may result in small movements that are negliable in the short term glacier dynamics, but can be important on geological timescales (Waller, 2001). Where the ice is at the pressure-melting point, sliding occurs more significantly. Several resistive forces act on sliding. First there is form drag, that comes from bumps and obstacles at the bed which ice must overcome by some mechanism. Second, debris attached on the bed ice which creates frictional drag. Ice flows past obstacles from two main mechanisms: regelation and enhanced creep.

The first theory of subglacial regelation was developed by (Weertman, 1964) and later modified by (Lliboutry, 1968, 1987; Kamb, 1970). As ice meets an obstacle, the pressure increases on the up-glacier side of it, lowering the pressure-melting point which encourages melting. The resulting melt water then migrates over the bump to lower pressure zones where it refreezes again due to the higher pressure-melting point there. The ice therefore bypasses bumps by temporally turning to water and back again.

The second mechanism that allows ice to overcome bed obstacles is enhanced creep.

It is important to recap from the flow law (equation 3), that the strain rate of ice varies non-linearly with the applied stress. Therefore, locally higher stresses on the upstream side of bumps causes the ice to deform and to a lesser extent bend over the obstacle. It should be remembered that creep rates are much lower for cold ice due to the temperature dependence from the flow law.

Which of the two mechanisms is most dominant depends on the size of the obstacle. Enhanced creep will be more efficient around large bumps, because a large volume of the basal ice experiences enhanced stresses and higher strain rates. As regelation is the dominate process around small objects, it follows that enhanced creep and regelation varies in importance relation to the obstacle sizes at the bed. An intermediate controlling obstacle size of 0.5 m, where both the mechanisms are equally inefficient and which presents maximum resistence to sliding was found by theoretical analyses and observations (Kamb and LaChapelle, 1964; Boulton et al., 1975).

Balance velocities

A glacier is typically divided two into distinct zones: an ablation zone and an accumulation zone, divided by an equilibrium line. In these zones mass is either lost or gained, respectively. The behavior of these areas explains the state of a glacier and is refereed to as the mass balance. Benn and Evans (2014) explained this simply by using the "wedge" concept, which reperesents mass gain or loss as two wedges (Sugden and John, 1976). The idealized glaciers in figure 1 show increasingly net accumulation values from zero at the equilibrium line to a maximum at the upper zone. Similarly, net ablation increases from zero to a maximum at the terminus. The rate at which mass is added or subtracted at the wedges is controlled by the mass balance gradient.

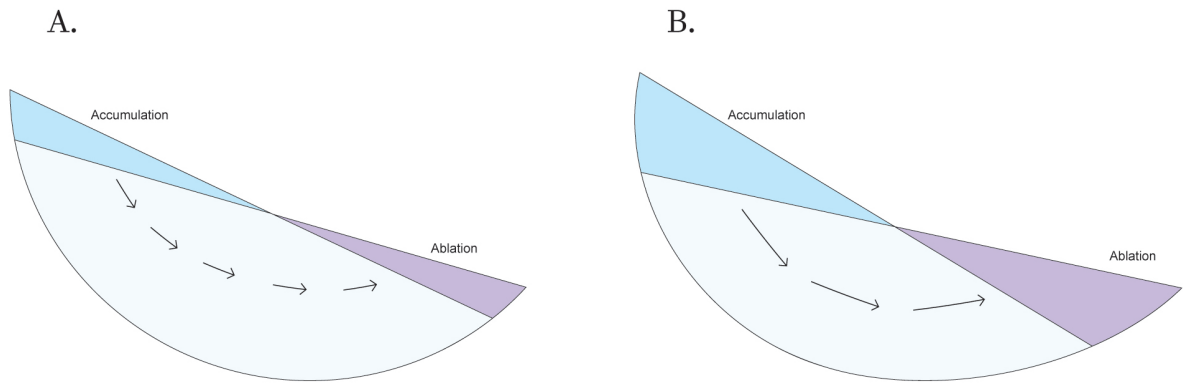

Figure 1: The figure shows the idea of balance velocities using the wedge concept. Modified from Sugden and John (1976)

To achieve a steady state, mass gained must be transferred to replace mass loss in the ablation zone, and ice discharge through any cross section on the glacier must equal the rate of net mass gain. Quantitatively, this can be expressed as:

$$Q_x = \sum_{i=1}^{x} \dot{b}_i w_i \tag{4}$$

Here Q_x is the discharge through a cross section at a distance x from the glacial head, b_1 is the net balance rate and w_i is the width.The average velocity through the cross section is:

$$\overline{u}_x = \frac{Q_x}{A_x} \tag{5}$$

where A_x is the cross-sectional area. Due to their dependence of mass balance, velocities calculated this way is referred to as balance velocities.

The role of water

Meltwater enters a glacier drainage system through a variety of ways. Internally, it may be produced at the surface from snow/ice melt, within the glacier from ice deformation causing friction between ice grains, and sub glacially from geothermal heating and basal friction. From extraglacial sources, water can directly come from rain, subaerial runoff or groundwater. Supraglacial melt is a major source of water, but varies spatially over the glacier's surface and in quantity through season(s). Englacial and basal melt is a steadier source of water, and varies more over long timescales. The controls meltwater has on glacial motion is dependent on supply, drainage and storage, and the connections

between subglacial, englacial and supraglacial systems.

Whether water flows over, through or below the glacier depends on the balance between the gradients in hydraulic potential and resistance to flow. In the case of water flowing on a surface, the hydraulic potential depends only on the waters mass and elevation. Predicting where it will flow is rather straight forward. The situation gets more complex within a glacier, because water can be affected by variations in pressure as well as elevation, which could result in vertical motion or whatever direction the gradient of hydraulic potential is moving towards to. This pressure however, is influenced by friction between the water and the walls which supports some of the overlying weight. This is referred to as resistance to flow. In channelized drainage systems, this is dependent on its dimensions and roughness properties, and through a porus media, on the size, tortuosity and connectedness of pore spaces.

There are several ways for englacial meltwater to connect with the bed. These connections are important as increased storage at the bed can trigger basal acceleration (Iken and Bindschadler, 1986; Willis, 1995). It was earlier thought that these connections could not occur on glaciers below the pressure-melting point, as cold ice would effectively act like a barrier to water flow (Hodgkins, 1997). However, such glaciers can exhibit dynamic responses to surface melt on short timescales, indicating water flow through englacial conduits, and has been observed on High Arctic glaciers (Boon and Sharp, 2003). There are several ways for englacial drainage systems to exist. Moulins (a circular, vertical well-like shaft which water enters from the glacier surface) form when supraglacial meltwater exploits a fracture on the surface which grow deeper from sustained water supply. Studies by Stenborg (1969) showed that moulins tend to develop at the up glacier end of crevasse field, were fractures captures supraglacial streams. Hydrofracturing occurs when meltwater enters crevasses and the water pressure acting on the walls overcomes the forces acting to close the crevasses. This allows water to rapidly propagate downwards, connecting the the basal plumbing network (Das et al., 2008; Stevens et al., 2015). Gulley and Benn (2007) showed that water can moved down to the bed by exploiting different permeabilities in the ice, such as debris filled fractures and crevasse traces. Englacially in temperate glaciers, water can also be stored in conduits, crevasses or fractured networks

as observed on Storglaciären by Fountain et al. (2005). On some polythermal glaciers, storage may occur in blockages of incised meltwater channels (Gulley et al., 2009).

Due to the profound influence it has on glacial dynamics, subglaical hydrology is one of the most important branches of glaciology. Here drainage systems can be subdivided into two main categories: channelized and distributed systems. Channelized drainage systems in the subglacial environment was first characterized by Röthlisberger (1972). Here it was argued that melt rates increase with water flux and thus water pressure will decrease with discharge, leading to the development of branching, in which large channels draw water from their surroundings. Channelized systems are characterized for representing an efficient drainage system as water is confined and can have high flow capacity Distributed systems extents over larger portions of the bed. These are associated with a thin water film between the bed and ice (commonly if the bed is hard) or as linked cavity systems, and characterized of their inefficient drainage capabilities.

Ice temperature

The role of ice temperature is an important part of glacier dynamics. In fact, it is so important that glaciers are categorized in terms of their temperature properties. To understand how it behaves in a big ice systems, such as on glaciers, it is necessary to understand the concept of pressure-melting point. The temperature at which ice melt is not constant at 0^oC but decreases as the ice is placed under increasing pressure at a rate of 0.072^oC per million Pascals (Mpa). Consequently, the melting point of ice is referred to as the pressure melting point. Glaciologists use a threefold classification on glaciers, all based on whether the ice is at or below the pressure-melting point: (1) temperate glaciers, which are everywhere at the melting point, except for the surface layer which is subject to seasonal temperature cycles; (2) cold glaciers, which are everywhere below the melting point and are frozen to their beds; and (3) polythermal glaciers, which are composed of both warm and cold ice. The most geographically widespread type of the three is polythermal glaciers and exhibits a wide range of thermal structures depending on the balance of surface and subsurface warming processes (Blatter and Hutter, 1991; **?**). These glacier types are further subdivided into predominantly cold and warm glaciers, six main types are commonly described and are presented in figure 2.

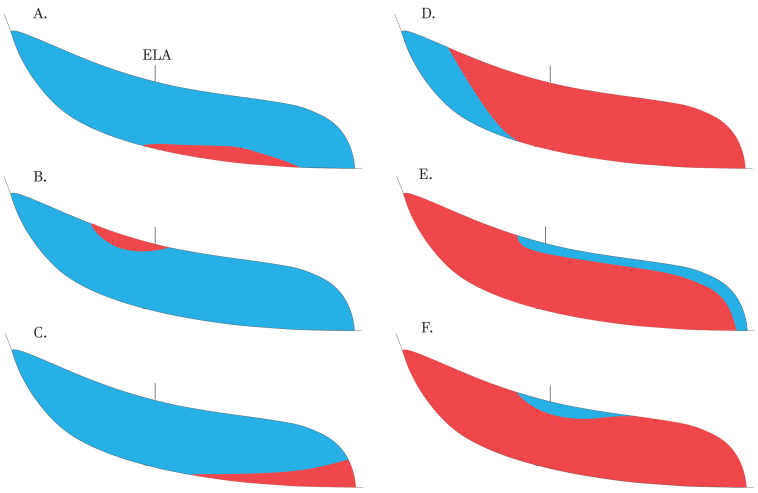

Figure 2: Main six types of polythermal glaciers, modified from **?**

Type (A.) and (C.) are mainly made of cold ice, but by depth strain heating subglacial ice can be raised to the pressure-melting point. In type (B.) the ice is predominantly cold where zones of warm ice can be present in near-surface areas. This occurs mainly from heat released by refreezing of meltwater and can also affect the ablation area. This forms in a similar way in type (D.), but cold ice is restricted to cold, high-altitude parts of the glacier. In type (E.) warm ice is created from refreezing of meltwater in the accumulation zone during spring. A near-surface layer of cold ice is present from chilling surface winds during winter. Polythermal glaciers of this type are commonly found in the polar maritime climate of Svalbard (Dowdeswell et al., 1984a). If the ablation rates are high, cold ice can be stripped apart from these area during summer melt (E.). Ice temperature and glacier flow are strongly interrelated. The relationship between them give several feedbacks important for glacier dynamics.

2.2 Glacial surges

Glaciers that switch between periodic phases of slow and fast flow is refereed to as surging glaciers. This process is a cyclic phenomenon which is not directly triggered by external events, but is internally driven from changes at conditions near the bed of the glacier (Meier and Post, 1969; Sharp, 1988). However, distinguishing between internal and external triggers is not that simple in some cases as internal factors are not fully independent (from external factors). Also, the wide spectrum of surge behavior can make the distinction between a fast moving non-surge and surge unclear (Meier and Post, 1969; Murray et al., 2003; Nolan, 2003; Frappé and Clarke, 2007). The period of slow motion between the active surge phase is refereed to as the quiescent phase. This period is commonly characterized with movement below the balance velocities, which causes ice mass gain in what towards/at the reservoir zone. The increase of mass in this zone and loss of mass in the ablation area near the terminus eventually causes a steepening of the glacier's longitudinal profile. As this continues, pulses of fast-moving ice can occur already several years before the surge (Kamb et al., 1985; Dolgoushin and Osipova, 1975). Closer up the onset of the surge, a clear front between the static ice down glacier and the increasingly active ice up-glaciers forms (Clarke et al., 1984). The front continues to steepen before the surge finally gets triggered Meier and Post (1969); Raymond (1987). During the surge, maximum velocities normally one or two orders of magnitude than in the quiescent phase (Benn and Evans, 2014). Within a glacier system, the duration of both phases tends to be somewhat constant, resulting in a quasi-periodic cycle. Between regions however, the length of the phases may has large variations (Dowdeswell et al., 1991).

Distribution of surge-type glaciers

For the last 100 years glacier surges have mainly been occurring within two super clusters. Firstly, in what is referred to as the Arctic Ring which includes Alaska-Yukon, Arctic Canada, parts of West Greenland (Disko Island and Nuusuaq Peninsula) and parts of East Greenland (Blosseville Kyst and Stauning Alper), Iceland, Svalbard and Novaya Zemlya (Post, 1969; Jiskoot et al., 2001, 2003; Copland et al., 2003; Fischer et al., 2003; Yde and Knudsen, 2007; Citterio et al., 2009; Grant et al., 2009) and secondly in the western central Asia including the Karakoram, Pamirs and western Tien Shan (Hewitt, 1969, 1998; Kotlyakov et al., 2008; Copland et al., 2009, 2011). Elsewhere, a smaller

portion have been observed in Cacasus, Andes, Kamchatka and Tibet (Kotliakov, 1996; Kotlyakov et al., 2004; Casassa et al., 1998; Espizúa, 1986; Wenjing, 1992; Dowdeswell and Williams, 1997; Dolgoushin and Osipova, 1975). Prior observations indicate that populations of surges may have migrated in the past through changes in climate patterns, fluctuating between surging and non-surge type glaciers. For example, a change in climate could result in insufficient mass accumulating to recharge the reservoir zone, leading to a transition from a surge to non-surge type glacier. This scenario was suggested by Dowdeswell et al. (1995) based on the contrasting 18 surge-type glaciers on Svalbard in 1936-38 compared with only 5 in 1990. Vernagferner in the Austrian Alps experienced four surge-like advances in the Little Ice Age, but seems unlikely to repeat this behavior (Hoinkes, 1969). Under other conditions, increased precipitation driven by climate change may have motivated higher frequency of surges seen in the Karakoram Mountains Hewitt (2007). Consequently, these observations suggest that it is possible for a glacier to undergo a single surge during a short-lived climate condition It also suggest, even though surges are internally triggered, that they are integrated in a wider set of controls on glacial behavior.

Between regions and within surge-clusters surge behavior can be very different. The most striking example is when comparing surge-type glaciers occurring on Svalbard and Alaska. Velocities are much higher in Alaska, which can move up to 50 m/d, compared to up around 20 m/d on Svalbard. Big differences also occur in the duration of the active phase. In Svalbard they are much longer, lasting between 4-10 years while in Alaska they are active for 1-3 years. In other parts of the world, there are a wide range of surge varieties also ranging between these two classes. In attempt to comprehend the distribution pattern of surging glaciers, a number of statistical studies have been done. This include comparing several distinct observations within and between regions, but finding a model capable of explaining all observed pattern does not yet exist. Still, detailed investigations have been carried out on very few surge-type glacier Benn and Evans (2014).

Surge models

Two main types of surges have long been defined in glaciology, which describe the triggering mechanism "that initiates the active phase". The first type, referred to as the "thermal switch" or "thermal instability" mechanism, is related to polythermal surges where subglaical conditions changes from cold to warm (Murray et al., 2000; Fowler et al., 2001). This explanation has a long history, and having been first argued by Robin (1955). During the quiescent phase glaciers are slow moving since the bed is frozen (at least in the lower glacier system) and ice mass starts to thicken the accumulation zone. Added mass increases the driving stress which leads to higher ice-creep rates. This increase in ice deformation caues heat and promotes a positive feedback between accelerating ice motion and strain heating. Eventually the ice connected with the bed rises to the pressure-melting point and any further energy generated from glacier motion is used to generate melt-water. Colder ice surrounding the melted water and the permafrost can prevent the water form escaping the glacier. This increases basal pressure which causes reduced basal drag and increased sliding. The surge propagates down glacier as stresses are transferred to the surrounding ice, causing further ice deformation, strain rates, and strain heating. In addition, injection of presssurized water along the bed and into the ice can also contribute significantly to surge propagation. A surge ceases when the water is able to escape the glacier, either through the bed or via thrusted faults extending from the bed to the surface.

The thermal switch is limited to polythermal glaciers, but Bindschadler et al. (1976) observed that temperate glaciers could also surge. This led to the development of the hydrological switch model. This type was first suggested by Röthlisberger (1969) and was emphasized also by Thorarinsson (1969) from the surges observed in Iceland. The model also includes water on the bed of the glacier, but as the bed conditions already are heavily influenced of meltwater, a surge occurs when the subglacial drainage system changes from efficient tunnels/channels to inefficient distributed networks. This model was mostly developed to explain observations of the 1982-83 surge of Variegated Glacier, and was further developed from other investigations on surging temperate glaciers (Kamb et al., 1985; Raymond, 1987; Eisen et al., 2005).

Surge behavior

Changes in glacier geometry, appearance and behavior indicate glacier surges. From observations of surge-type glacier in the Canadian High Arctc and on Novaya Russian Arctic, Copland et al. (2003) and Grant et al. (2009) put together a comprehensive list of glacial features that are regarded as indicators for surge glaciers. These include: (a) looped medial moraines, formed as active-phase surge-type glacier flow past their neighbouring glacier and deforming the medial moraines between them; (b) ice foliation; (c) a change toward enhanced crevassed surface; (d) potholes on the glacier surface during the quiescent phase; (e) a rapid terminus advance; (f) shear margins on the glacier surface in the boundary between fast-moving surging ice and slower non surging ice; (g) rapid increase in surface velocities and (h) digitate terminus (in tidewater glaciers). Most of these glacial features can occur in a non-surging glacier, but the presens of many features together are indicative of surge behavior. The cleares evidence of a surge is an increase in surface velocities. This dramatically enhances crevasses in the ablation zone (Meier and Post, 1969). Elevation change is another propertiy of surge glaciers, in particular a thickening in the frontal zone and up-glacial thinning (Meier and Post, 1969; Melvold and Hagen, 1998; Nuth et al., 2010). Changes in the surface elevation is also typical during the quiescent phase of glacier, where a steepening along the longitudinal profile is common. On Svalbard this has been detected on several surge-type tidewater glacier such as Comfortlessbreen, Aavatsmarkbreen and among other (King et al., 2016; Sevestre et al., 2018). Advancing of the glacial front can be an indication in some cases, but not all surges show a significant advance (Braun et al., 2011; Mansell et al., 2012).

3 Aim for this project

In this thesis we investigate Negribreen, a surge type tidewater glacier located on the eastern coast of Svalbard. In 2016 the frontal zone of the glacier collapsed and the onset of high velocities was detected from satellite imagery. By accessing remotely sensed data, this study explores the glacier's surface evolution since 1969. To achieve this, detailed analyses are executed through surface elevation and ice horizontal velocity data sets, and mapping its terminus positions among other structural surface changes. This thesis aims to derive and discuss possible triggering factors resulting in the collapse and compare observations to other surging glaciers on Svalbard.

4 Study site

Negribreen is a polythermal tidewater glacier located mid-east on Spitsbergen, Svalbard (figure 3). A section of Lomonosovfonna and Filchnerfonna are its reservoir area, connected to the glacier through Opalbreen and Filchnerfallet, respectively. Its terminus outlets into Storfjorden in Olav V and Sabine Land along with the neighbouring glaciers Ordonnansbreen, Akademikarbreen and Rembebreen. Between these tributaries, there are distinct medial moraines. These glaciers, along with some other make up the Negribreen glacier system. All together it covers an area of 1.180 km^2 which makes it one of the biggest glacier systems on the Svalbard Archipelago (Ottesen et al., 2017a).

According to the bedrock map from Dallman (2012), the western parts of the glacier system, the bed consists of old Neoproterozoic rock . This includes formations related to the Polaris and underlying Akademikarbreen geological group (orange and light blue box figure 3, respectivly) and marks a transition from predominatley carbonate to mixed carbonate-clastic sedimentation (Arnaud et al., 2011). Slightly eastwards, there are younger bedrocks from Permian period. Firstly from the Gipshuken formation (light green box, figure 3), which is composed of rhythmic sequences of limestone/dolomite, anhydrite and carbonate breccia (Harland, 1997). This formation is often associated with gentler slopes covered by broken rock fragments. Overlying this is the Kapp Starostin (dark green box, figure 3) formation consisting of chert, siliceous shale, sandstone and

limestone. As apposed to the Gipshuken formation, these bedrocks commonly form cliffs associated with steep canyons and waterfalls (Mørk et al., 1999).

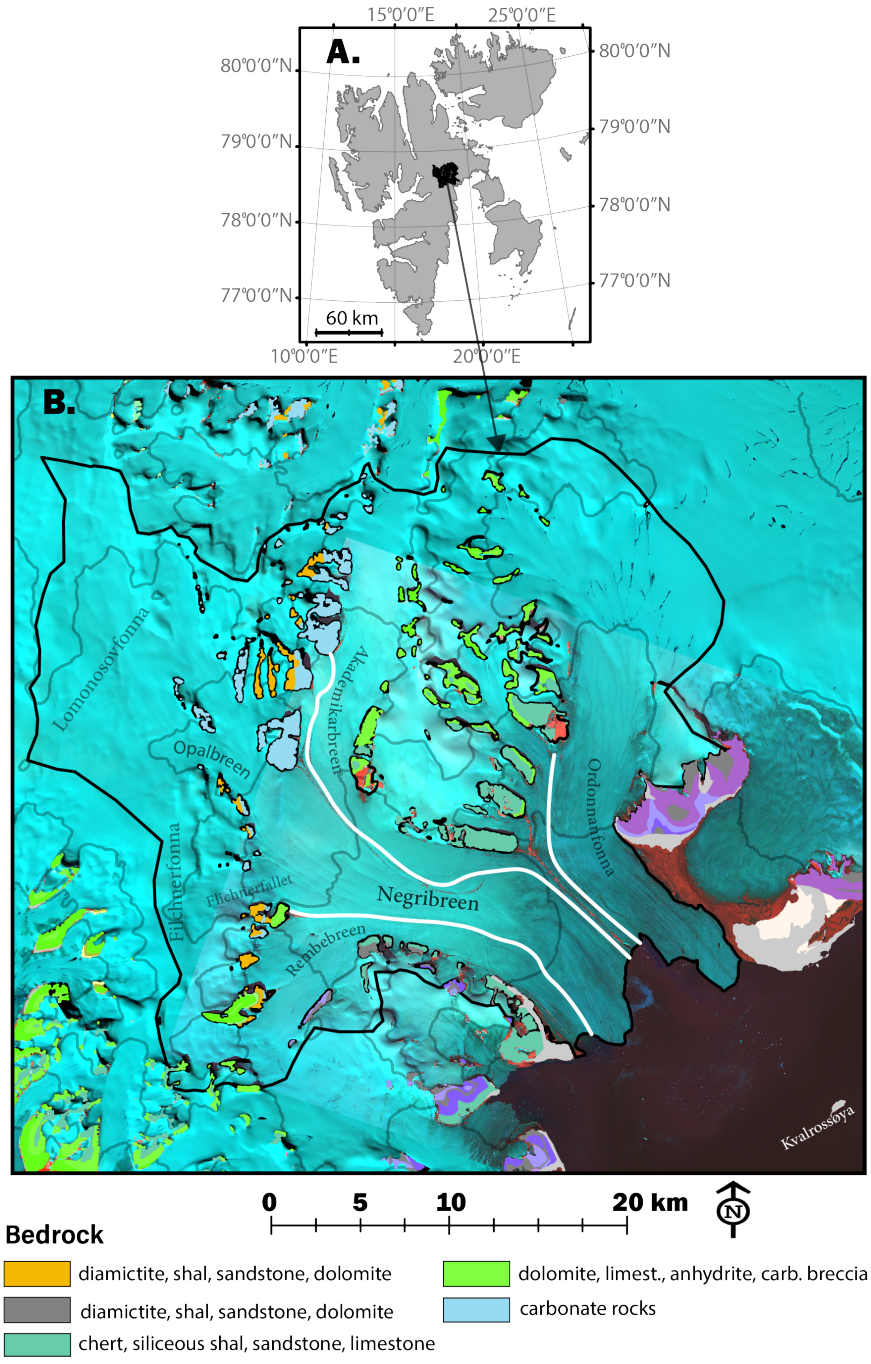

Figure 3: Study site overview where: A. shows location of Negribreen's glacial system on a map of Svalbard and B. detailed display of Negribreen and its neighbouring glaciers, overlayed with color-coded bedrock (legend only from within the glacier system), 200 m contour-lines (gray lines) and medial moraines (white lines). The underlying image are from a Landsat-8 optical imagery in 2015-08 consisting of band 7, 5 and 4., bedrock consist of generalized large-scale data (1:100 000, 1:50 000) by Dallmann W. K (2002-2012)

4.1 Previous observations

Historically there is a lack of field-based study on Negribreen and as a consequence, dynamics is poorly documented compared to other glaciers on Svalbard. From older expeditions along eastern parts of the archipelago, many previous observations include information about its terminating position. Combined with some input from aerial imagery in the 1900s, Lefauconnier and Hagen (1991) gathered these observations by creating a map showing its evolution in glacier extent (figure 4). The earliest observation are from von Heuglin (1872) where Kvalrossøya (an island located at the coast where Negribreen terminates) was not observed and was pressumed to be overridden by the glacier. In 1899 several expeditions walked on the northern side of the glacier. A map from Wassiliew (1925) from this time recorded a small moraine island, which very likely is the island of Kvalrossøya. Photographs from this expeditions also showed moraines which indicate the glacier was in regression. Photographs from 1936 show a significant advance in terminus position compared to measurements taken by Gripp (1929) in 1927. Kvalrossøya was not visible in these photographs, indicating the glacier was surging at this time. Aerial photographs from the upper accumulation areas to Negribreen, Akademikarbreen and Ordonnasnbreen all showed crevassing and suggesting that most of the glacier system was contributing to the terminus advance (Lefauconnier and Hagen, 1991). Between 1935-36 the average rate of the front positions was calculated to be 35 m/day (Liestøl, 1969). On a recent bathymetry survey on sea-floor morphology in eastern Svalbard, moraines from that event along with other depositional structures. The terminal moraine formed by the surge event shows most likely the largest extent of Negribreen during Holocene, since the sea-floor beyond is largely smooth and fine-grained Ottesen et al. (2017a). After the surge event, areal images have shown little signs of fracturing on the glacier surface and the front has showed to be in continuous retreat (Lefauconnier and Hagen, 1991).

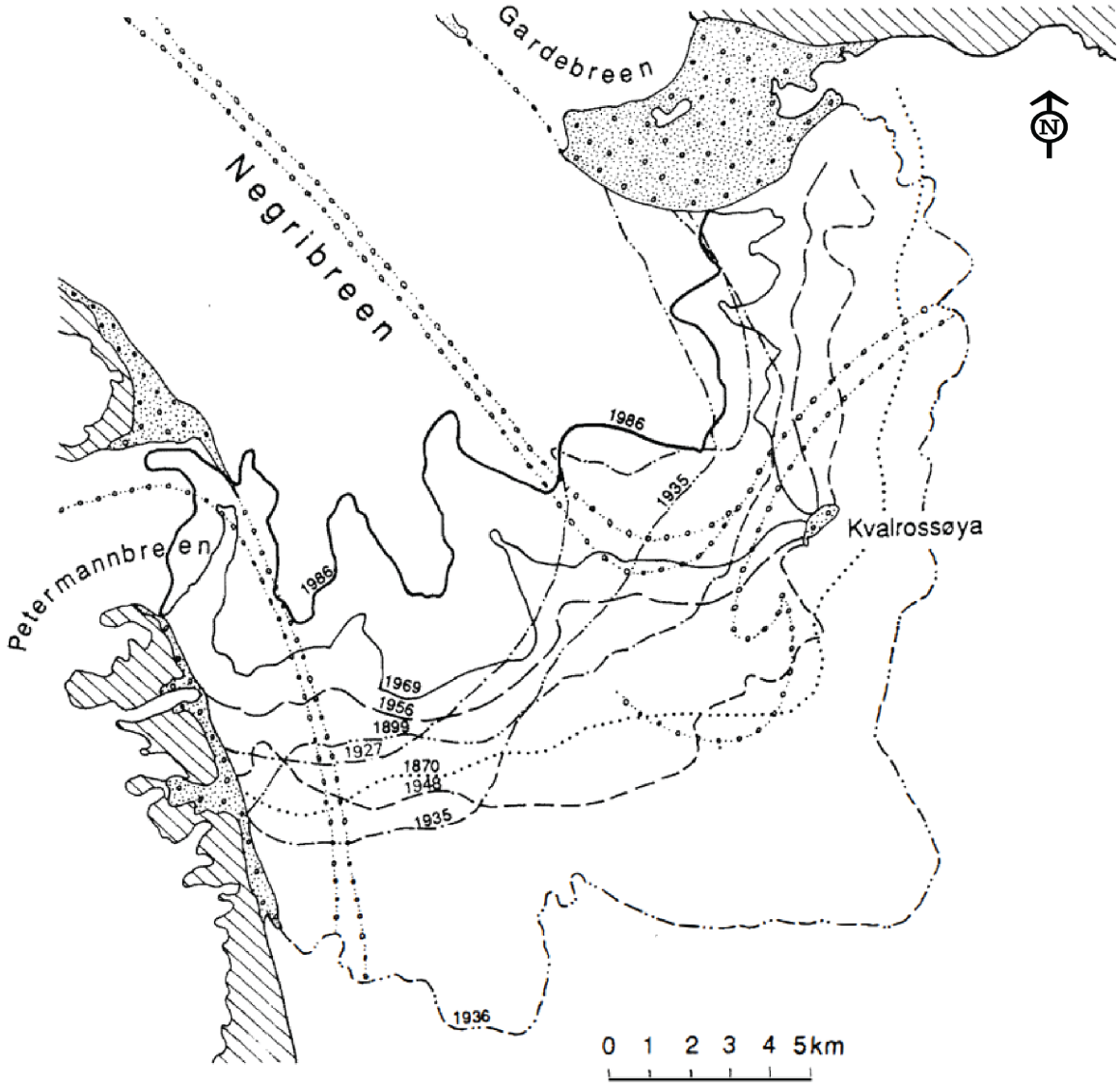

Figure 4: Map showing historical front positions on Negribreen, by Lefauconnier and Hagen (1991)

5 Data and methods

5.1 Horizontal ice velocities

There are two main techniques for detecting of glacier movement from remote sensing data; image matching and differential interferometric synthetic aperture radar (DInSAR). Both methods complement each other because they work over different time spans in glaciological studies. Image matching is applied over time spans from weeks to years, and DInSAR from days to weeks. In this study, horizontal ice velocities have been obtained from both methods.

Image matching

Image matching, correlating images containing the same objects, is used in several different fields such as photogrammetry, image mosaicking, map updating, and tectonics among other application. In glaciology, this is widely used to detect ice movement. There are different mathematical ways to find the best correlation between two images (Kuglin and Hines, 1975; Leprince et al., 2007). On the data used in this study, a algorithm called normalized cross-correlation (NCC) was used. NCC is a matching method that is very common when studying glacier velocities. The principal of the NCC method are shown in figure 5. The earliest image (acquisition 1) is taken as a reference, and a window of this image is correlated over a subset of the latest image (acquisition 2). The peak of the cross-correlation surface indicates the displacement between the images.

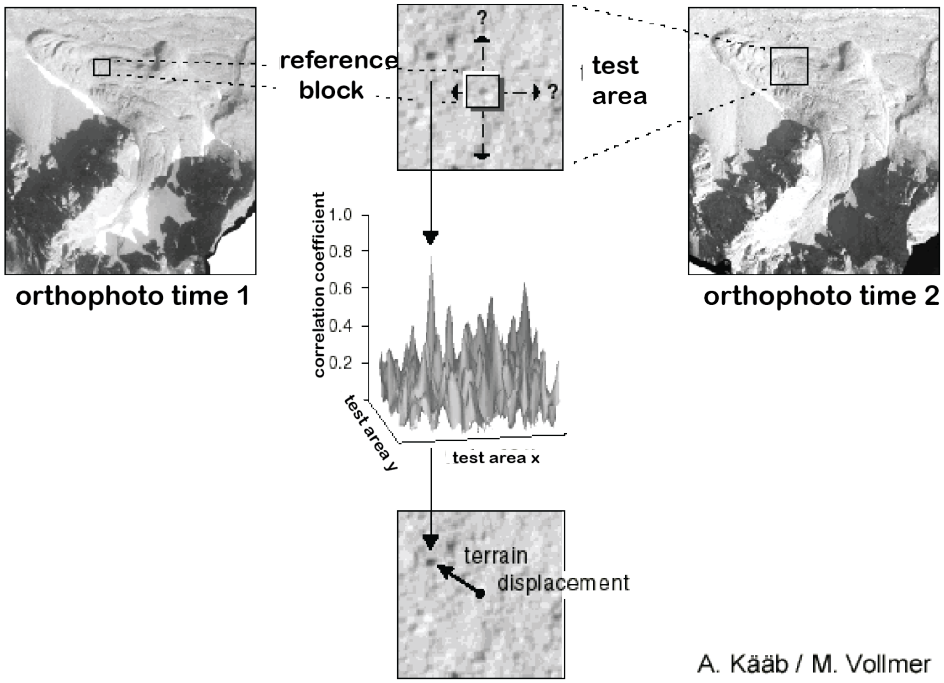

Figure 5: Principal figure of how image matching through normalized cross-correlation finds the terrain displacement. From Kääb (2005)

Image matching can be applied on optical and radar images and in both cases the purpose is to recognize features such as crevasses, debris and among other structures over both images to derive velocity. A major complicating factor in optical image pairs are their vulnerability to clouds and reliability of sufficient daylight. This especially affects high Arctic maritime environments such as Svalbard, where most days are cloudy and winter months bring the polar night. Images also need to contain visual contrast, and this further limits optical data to mainly be used in the ablation area of glaciers when snow-cover is absent. Due to polar night the application of optical imagery is only available during spring, summer and autumn. In contrast, radar images are created are not dependent on daylight and they also penetrate clouds and are an important source for monitoring during winter months. To document velocities throughout the whole year and achieve necessary temporal coverage on Negribreen, data sources from several satellites including both optical and radar sensors. When there is sufficient daylight, we mainly use velocities derived from Landsat-8. Where there are major gaps or a need for higher temporal resolution data, additional velocity fields are added from Sentinel-2. During polar night or in transitions to winter, data is derived from Sentinel-1. Figure 6 show

where velocity data was extracted on Negribreen.

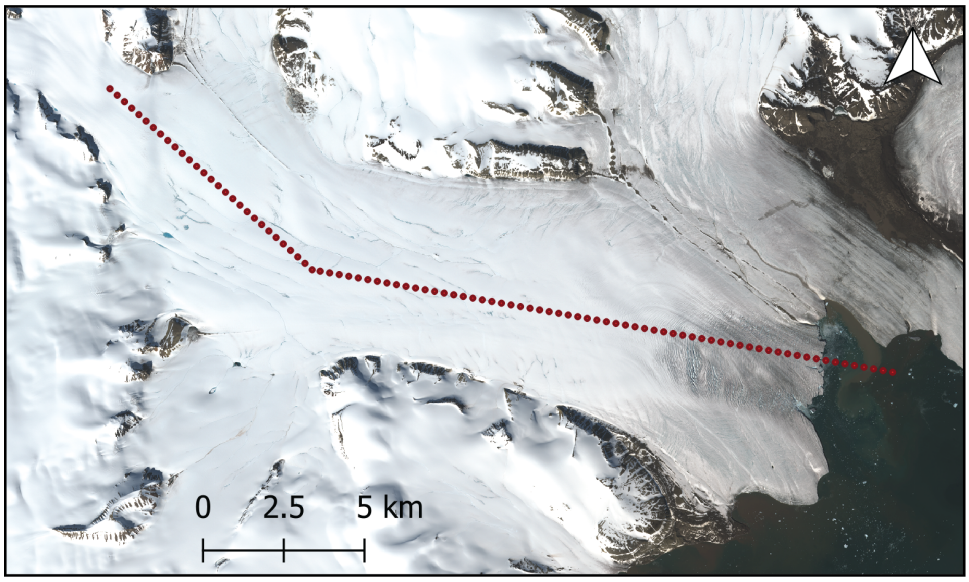

Figure 6: The velocities were measured in points with a 300 m spacing along the center of Negribreen (dotted line).

Velocity data from Landsat-8 was extracted from the Global Land and ice Velocity Extraction (GoLIVE) (Scambos et al., 2018). The data sets are publicly open through NSIDC File Transport Protocol site. These velocity fields are created by finding displacement between image pairs from the panchromatic band with 15 m resolution. Normalized cross-correlation is applied between the image pairs on a sampling grid of 300 meters spacing. More information about the GoLIVE project: https://nsidc.org/data/golive

All data covering Negribreen including grid locations having a path between 209-219 and row of 003 or 004 (Landsat-8 path/row grid system) were analyzed. In total this makes up 84 data files. All grids were reprojected to WGS 84 / UTM zone 33N. The velocity maps were spread between 2014 to 2018, but most of the data come from 2017 and 2018. Only the highest temporal resolution (16 days) repeat cycle was used. Among the data variables included in the NetCDF files we extracted the masked magnitude of velocity and peak correlation value. A code using MATLAB was created which looped through all velocity files and extracting pixels with 300 m spacing along a centerline 6, having a correlation $\leq$0.3 (values range from 0-1). This correlation value was chosen

as it seemingly gave the best relationship between noise and "correct" velocities, where most noise was distinct and could be manually removed. Although a higher correlation of e.g.≤0.6 would give less noise, it would also filter out some correct velocities in the process (figure 7).

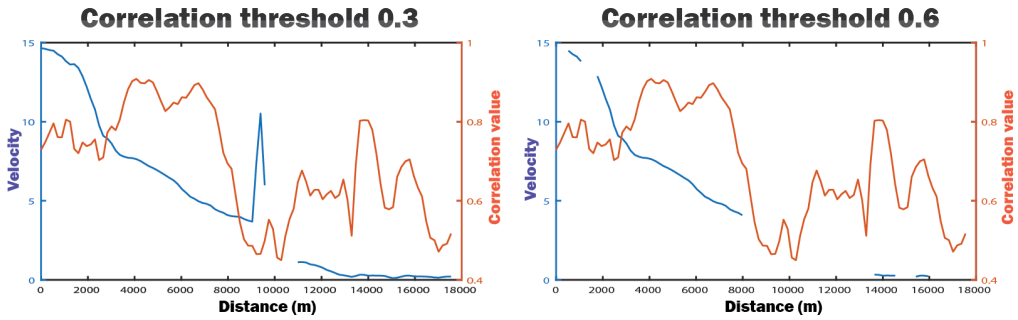

Figure 7: The figure compare two different correlation values on the GoLIVE velocity data and highlights the importance of choosing a correct value. Here a correlation of ≤0.3 is compared with a value ≤0.6 and is a better alternative because less correct values are masked out and noise are still easily detectable.

Velocities from Sentinel-2 were used to supplement Landsat-8 data. Data were provided by Bas Altena (personal communication), created by the framework of Altena and Kääb (2017). A total of 246 partly cloud free images from the Sentinel-2 archive was used during sun-lit days in 2016, 2017 and 2018. Sentinel-2 is a twin satellite constellation and combined acquisitions coverage resolves in a repetition rate of 5 days at equator. This rate increases due to convergence of orbits towards the poles and consequently makes across-track photogrammetry possible (Altena and Kääb, 2017). Displacements were matched between all possible pairs of images within 100 days separation. Of these 8 velocities field where used in this investigation with ≤ 10 days image separation.

Sentinel-1 comprises a constellation of two polar-orbiting satellites which operates day and night. They actively perform imaging with a C-band synthetic aperture radar, enabling them to acquire imagery regardless of weather (Yagüe-Martínez et al., 2016). A total of 15 image pair was downloaded through Sentinel open access hub:`https://scihub.copernicus.eu/dhus/#/home`. Velocity fields were generated by using the Sentinel Application Platform (SNAP) and following the steps presented in figure 8.

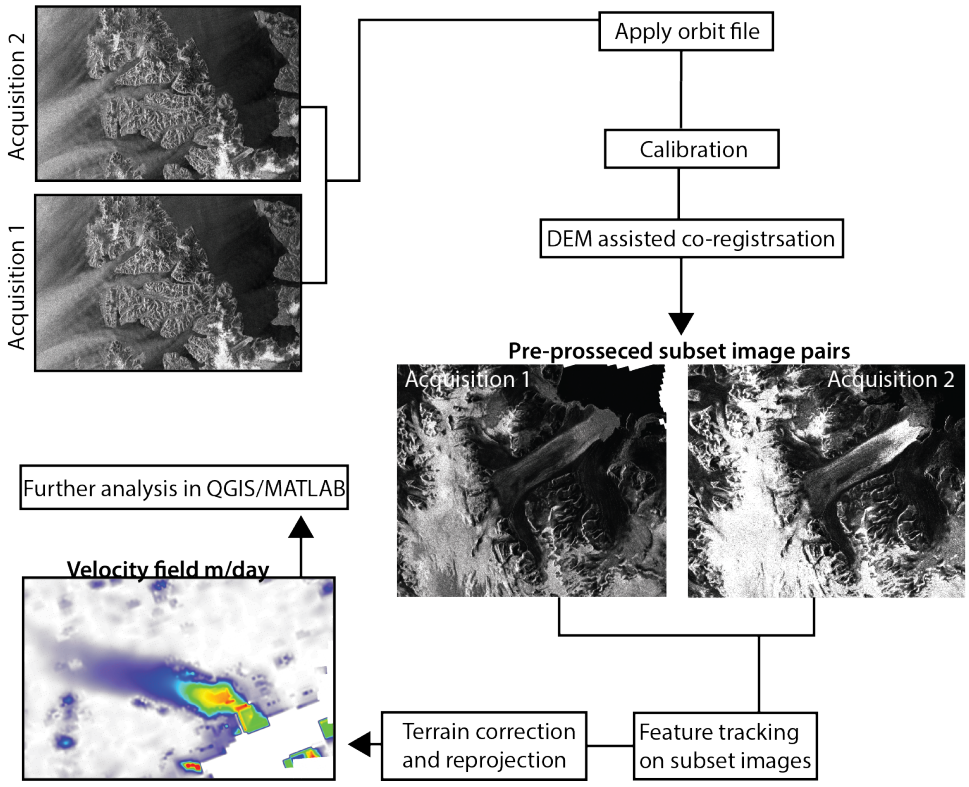

Figure 8: Flow chart showing the steps for extracting velocities from a Sentinel-1 image pair

The image pairs require pre-processing before feature tracking can be applied. This includes accurately positioning both images, first individually by including orbital files and then align them by co-registering with a DEM. Since SAR data does not include radiometric corrections the images were calibrated so the pixel values truly represent the radar backscatter. After pre-processing, image matching through NCC was done on a subset view of the images to minimize processing time. Window dimension was determined to be 300 meters in both azimuth and range spacing, this was found by assuming maximum velocities 18-20 m/day. This makes the search box large enough so that texture and not noise is matched but also not too big which complicates the matching when there is much deformation.

Interferometric Synthetic Aperture Radar

To obtain velocities from earlier periods, we were able to get a snapshot from the European Remote Sensing (ERS) satellites in 1995. When both was active, the ERS satellites observed the Earth at nightfall on ascending tracks and at dawn on descending track (Scharroo and Visser, 1998). An image pair from this tandem constellation was processed

and directly provided by Thomas Schellenberger (personal communication). The velocities are created using interferometry by comparing two separate snapshots acquired at distinct points in time. In principal, when the satellite has its pass over a location it actively sends out radar waves towards the ground and when transmitted waves hits the surface they reflect (backscatter) and get collected by the satellite sensor (pass 1). During a subsequent orbit, another collection of radar waves gets measured from the same orbital location (pass 2). Surface motion can be detected by comparing the phase of the coherent radar signals from pass 1 and 2. If the surface has moved, the collected radar waves from pass 2 will not match with pass 1 and be "out of phase". All wave differences can be converted into the component of ground-motion along line-of-sight to the satellite (either towards or away from sensor), where higher contrast in phases translates to more movement. Since the change in phase also include movements in the z-direction, a digital elevation model needs to be subtracted to get true horizontal velocities.

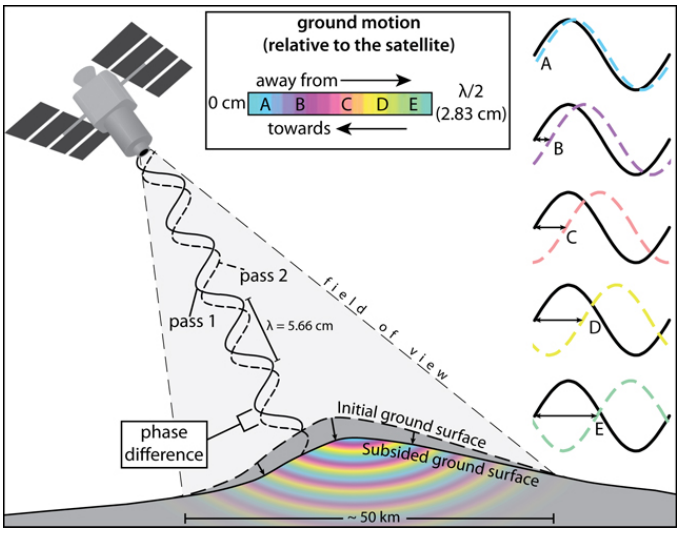

Figure 9: Principal figure of how interferometry can be used to measure ground-motion by comparing phase differences between two satellite passes. In this example, interferometry is used to detect change after a volcanic deformation process. Figure from: Smithsonian Institution

5.2 Elevation data

Digital Elevation models (DEMs), are digital files consisting of points of elevations, sampled systematically at eaqually spaced intervals relative to a datum, and referenced to a geographic coordinate system (Sanli and Abdikan, 2006). For studying glaciers, changes in surface elevation give important information about their dynamics, and are accessible through various remote sensing platforms. On Negribreen, we investigate the rate of surface change since 1969 by differencing between multi-temporal elevation models. To calculate the rate of change (Δc), an older elevation (e) are subtracted by a new and divided by the time separation (Δt), see equation 6.

$$\Delta c = (e_{new} - e_{old})/\Delta t \tag{6}$$

The elevation data we used for this analysis was collected from several sources, as listed in 1, and each elevation product was resampled and differenced with its closest year, with exception of 2014. These were only differenced with the 1990 DEM.

Table 1: The table list a overview of all elevation products used in this study and their co-registration results (x, y and z shift, Root mean square error and number of iterations). The resolution are their resampled values.

Data types	Date	Type	Res(m)	Δx	Δy	Δz	RMSE	iter
Norsk Polar Institutt	1969	aerial	20	0.0	-0.2	0.0	5.1	2
Norsk Polar Institutt	1990	aerial	20	-0.4	-0.1	0.0	5.0	2
ASTER	7. July 2004	Stereo.sc	30	0.4	0.6	0.3	10.3	2
TanDEM-X	≈winter 2011	Int.fer	36	0.2	-0.2	0.0	4.6	2
Arctic DEM Strip	22. April 2014	Stereo.sc	40	0.0	-0.2	0.0	2.3	2
Arctic DEM Strip	24. April 2014	Stereo.sc	40	-0.1	0.0	0.0	1.7	2
Arctic DEM Strip	12. July 2015	Stereo.sc	40	0.0	0.0	0.0	1.5	2
Arctic DEM Strip	30. July 2015	Stereo.sc	40	0.0	0.1	0.0	3.6	2
Arctic DEM Strip	22. July 2016	Stereo.sc	40	-0.1	-0.1	0.0	2	2
Arctic DEM Strip	3. August 2016	Stereo.sc	40	0.0	-0.1	0.0	2.4	2
Arctic DEM Strip	22. May 2017	Stereo.sc	40	-0.3	0.3	0.0	2.4	2
Arctic DEM Strip	30. May 2017	Stereo.sc	40	0.0	0.1	0.0	1.7	2
ASTER	14. August 2018	Stereo.sc	30	0.6	0.1	0.1	8.2	2

Most of the products were stereoscopic DEMs, which are generated from along track

stereo imagery and uses the principals of photogrammetry. Here, measurement of the apparent positions on the images gives the difference between the projected stereo rays of the same object onto Earth's surface, and by knowing the camera positions, the sensor look-angles and camera parameters this can be converted to height (Lillesand et al., 2014). This method applies for the data acquired in 2004 and 2018 from The Advanced Spaceborne Thermal Emission and Refelction Radiometer (ASTER) and 2014-2017, data from Arctic DEM strip files. The ASTER satellite has for 20 years collected stereo pairs on a global scale (Girod et al., 2017). The optical imaging system has a ground swath of 60 km. It contains a nadir and backward VINIR sensor (Visible and Near Infrared) within the 0.76-0.86 μm range of the electromagnetic spectrum, whereas both sensors are seperated by $\approx 30^{\circ}$ which corresponds to a B/H ration of 0.6 (Toutin, 2008). Arctic DEM is a constructed by in-track and cross-track imagery from the DigitalGlobe constellation. The constellation is a commercial satellite imagry company and operates optical earth imaging satellites (WordView1, 2, 3 and 4, QuickBird, IKONOS and GeoEye-1). The strip files corresponds to the overlapping area of the input stereo image swath as they are collected by the DigitalGlobe polar orbiting satellites and are provided with a 2 m resolution (Porter et al., 2018). As the strip files were too narrow, two separate files with close acquisitions were merged.

Products from 1969 and 1990 were created from aerial surveys by Norwegian Polar Institute (2014). Similar to the stereoscopic DEM, they are created by the principals of photgrammetry. The DEM from 1969 did only cover the lower ablation area on Negribreen, which limited the information during this time.

The TanDEM-X, operates in a tandem with the TerraSAR-X satellite where they follow an orbit track separated by 500 m for each other. DEMs are created from the principal of interferometry, similar to how horizontal velocities are extracted from the ERS satellites 5.1. One satellite transmits radar signals and both records the amplitude and phase from the backscatter signals. Each pulse of radar transmits with minimal intervals, resulting that the receiving signals only reflects elevation and not other on the surface (Lillesand et al., 2014). Data acquired from this platform are from winter 2011, but its radar capabilities results in snow cover being penetrated (Dehecq et al., 2016).

This causes a displacement of the interferometric phase center to be below the surface, resulting in a negative bias between the actual surface. Therefore we conclude that the TanDEM-X data on Negribreen reflects summer 2010 elevations.

All DEMs were co-registered and provided by the supervisors of this thesis (Christopher Nuth and Robert McNabb) so that we could achieve unbiased elevations changes. this type of glacial studies a universal co-registration methodology was created by Nuth and Kääb (2011). They propose a three-step statistical framework for correcting the data related erros and include; (1) remove DEM shifts in the x an dy direction, (2) check for elevation-depended biases (z direction), and (3) biases related to aqusitions geometry of datasets. Before applying this methodology, all DEMs need re-sampling to the same spatial resolution and projection on the same coordinate system. To calculate unbiased elevation changes, errors are corrected and quantified first over stable terrain (off-glacier). For this its required a consistent mask for determining the stable terrain covering the study site. Over eastern Svalbard stable terrain mostly includes nunataks between glaciers and along the strandflats (Hisdal, 1985). The shift between x and y direction are corrected by using the relationship of elevation differences with terrain slope and aspect (terrain orientation). This is done iteratively over the stable terrain until the magnitude of the vectors are less than 0.5 m and then same corrections are applied to pixels in the un-registered DEM.

The co-registration process was in reference with the ArcticDEM mosaic dataset, which has consistent data and good coverage over stable terrain in the arctic. All DEMs had 2 iteration which gave aceptable results as shown 1. The final root-mean-square error (RMSE) show highest accuracy on the ArcticDEM strips datasets which gave mostly below 2.5 m error, with exception from 30. July 2015 that had 3.6 m. The ASTER scenes have the lesat accuracies with RMSE 10.3 and 8.2 in 2004 and 2018, respectively. Nuth and Kääb (2011) suggested that higher shift magnitudes in ASTER scenes could reflect less accuracy in satellite positions and sensor angle information. Possible because its been orbiting longer. It could also reflect its stereo configuration og having a base-height ratio of 0.6.

5.3 Glacier length change

General trends in glacier extents were measured since 1969 until 2015. Images were acquired from Landsat-1, landsat-5, Landsat-7, Landsat-8 and downloaded from `https://earthexplorer.usgs.gov/`. A more detailed measurements were taken between 2016-2018, covering every December and June from Sentinel-1 and Sentinel-2, respectively (table 2).

Table 2: The table list all the images used for measuring the front positions on Negribreen. The image from 1969 is the same co-registered data file from section 5.2

Period	Source	Res (m)
1969	Norsk Pol.inst DEM	20
1979	Landsat-1	60
1990	Landsat-5	30
2004	Landsat-7	30
2010	Landsat-7	30
2015	Landsat-8	15
June 2016	Sentienl-2	10
Dec 2016	Sentinel-1	10
June 2017	Sentinel-2	10
Dec 2017	Sentinel-1	10
June 2018	Sentinel-2	10
Dec 2018	Sentinel-1	10

Ice front positions were mapped between image pairs by adapting the "box method" as seen in Moon and Joughin (2008) and Howat et al. (2010). This method yields a less arbitrary measure of front positions than the change along a line(s). Here a box with a fixed width (W) is placed over the glacial extents along the flow direction. The outline of the front position on each image is then manually digitized within the lateral borders of the box (figure 10 A). Between two outlines of an image pair the total area (A) is measured. The average change in length (L) of the terminus was then calculated according to equation 7, and thus the rate (r) is calculated from equation 8.

$$\Delta L = \frac{A}{W} \tag{7}$$

$$r = \frac{\Delta L}{\Delta t} \tag{8}$$

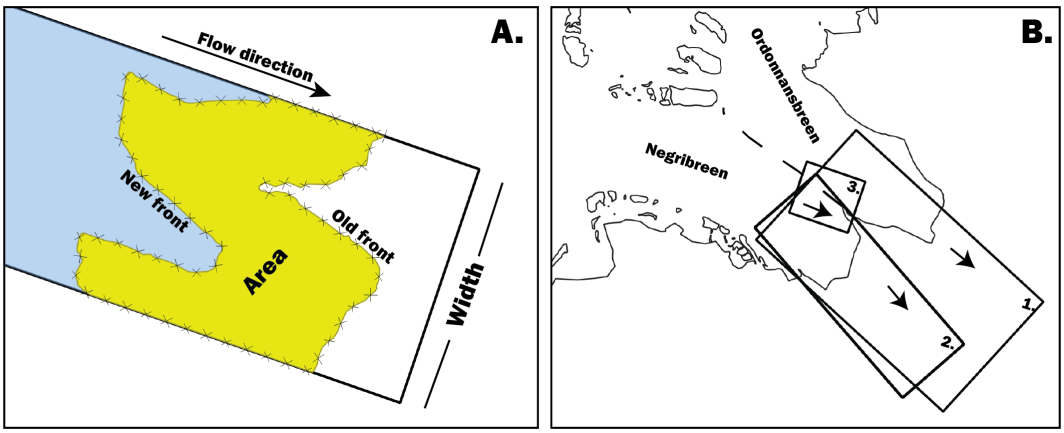

Figure 10: A. Principal figure of the Box method. A box are placed along the flow direction. The area of change between two front positions gets manually digitized (yellow area) between the walls of the box and divided by the box width. Rate of change is found by further dividing on time. B. Shows location of the three boxes used in this analysis. Both Box 1. and Box 2. calculate front positions between intervals within 1969-2015 on Negribreen and Ordonnansbreen combined, and on Negribreen alone, respectively. Box 3. calculate the recent terminus positions on Negribreen between intervals within 2016-2018.

Before applying this method, there were two considerations that needed to be accounted for. First, the coastline to where Negribreen flows makes it difficult to chose a fixed box angle. This is because the wide and open geometry of the fjord highly influences flow direction of the ice (depending on the glacier extent). Secondly, the terminus to Negribreen relations with Ordonnansbreen, which makes a box with a fixed width inaccurate as the intersection between the glaciers most likely fluctuate over time. To minimize inaccuracies related to these issues there were crafted three boxes (figure 10 B). Box 1 and 2 were used when measuring ice front position between 1969 and 2015 where; Box 1 has a width covering both Ordonnansbreen and Negribreen with a tilt reflecting a generalized flow line of the glaciers and Box 2 with a width representing only Negribreen with a tilt indicating its flow direction. A smaller Box 3 was used for the recent measurements between 2015 and 2018.

It was found that image scenes from Landsat-1 and 5 had significant shifts in the x and y directions and some shifts was also noticed on the Landsat-7 images. This error was improved by creating ground control points (GCPs) and geo-referencing them to fit a Landsat-8 image, which is believed to be more accurately orthorectified. A collection of five GCPs were distributed along the coastline over recognizable stable terrain. To get an idea of the inaccuracies remaining after the alignment, outlines of Kvalrossøya from the different images was compared with an image from Landsat-8 (figure 11). The outline from Landsat-1 appears larger due its bigger pixel dimensions. In the 1990 image sea ice made it difficult to see a clear boundary which possible explains a more narrow outline. There still seems be rather large inaccuracies in the 2010 image with a shift in the x direction between 50-110 m.

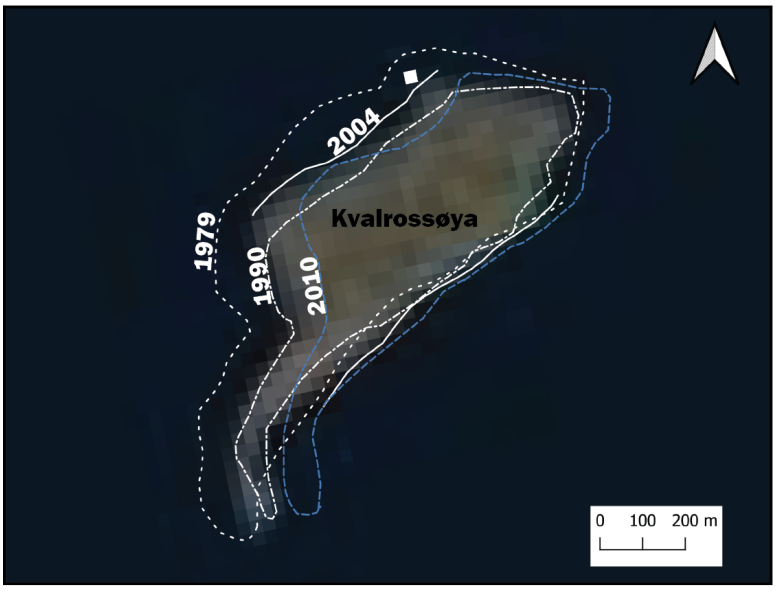

Figure 11: The figure compares outlines of Kvalrossøya after co-registration from the poorly aligned Landsat-1 (1979), Landsat-5 (1990), and Landsat-7 (2004 and 2010) images with a correct Landsat-8 base map. This highlights that there still is remaining errors in the horizontal direction, especially in images from 1979 and 2010. The whole outline from 2004 does not show due to the striping effect from Landsat-7

Another issue causing errors in this analysis are related to manually selecting delineation of the front positions. This uncertainty affect especially the mapped front positions from Landsat-1 in 1979, Landsat-5 in 1990 and Landsat-7 in both 2004 and 2010. Although the image from Landsat-1 had a distinct intersection between the glacier and sea ice, but its low pixel resolution of 60 m caused a persistent limitation in accuracies

along the intersection boundary of 2-3 pixels (figure12 A). On the Landsat-5 image, the increased pixel resolution to 30 m improved the ice front delineation where the glacier front was clear. However in some areas it were difficult to distinguish between icebergs and the glacier front. Also some areas was characterized with shadowing and poor contrast between the front and sea ice (figure 12 B). The Landsat-7 images are affected by stripping because of the failure of its scan line corrector in 2003. The complication of this effect was more significant where the shape of the glacier front was paralleled with the stripes. Where this occured the front delineation was assumed to be along the middle of a stripe (figure 12 C).

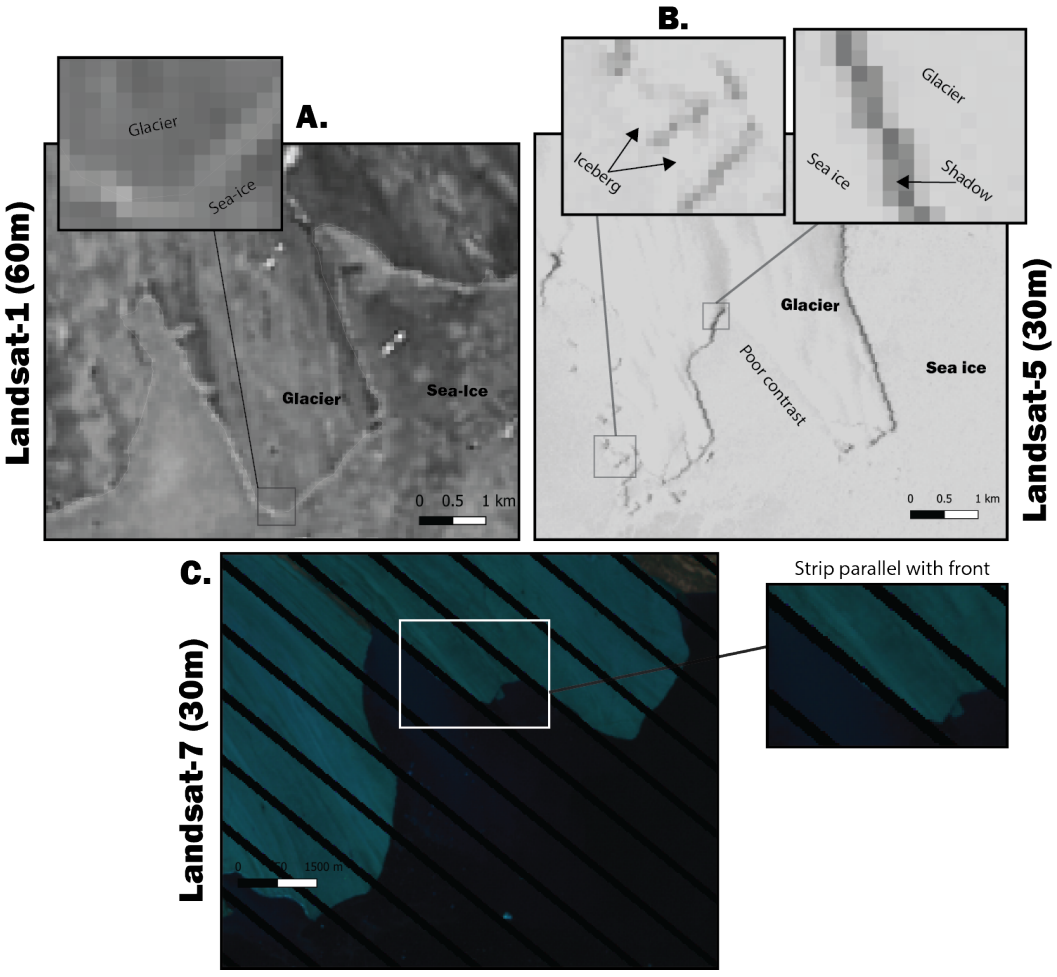

Figure 12: The figure highlights common errors related to when manually delineate the glacier front position. A. Landsat-1 image where most uncertainties was a results of its poor pixel resolution of 60 m. B. Errors related to Landsat-5 was from ice bergs, shadowing and poor contrast due to sea-ice. C. Shows the striping effect occurring on Landsat-7 images. The stripes caused most uncertainties where they were parallel to the glacier front (see outcrop).

6 Results

6.1 Velocities

The earliest velocity snapshot from remote sensing comes from the ERS 1-2 Tandem which provided interferometric precision. Remark however, that detection of glacial movement is only based of the satellites "look-direction". Still, data acquired in 1995 show there are paths on Negribreen's glacier system that show higher velocities. This is shown clearly Lomonosovfonna, where there are three paths with higher movement. They all connect to Negribreen through Opalbreen, an area experiencing the highest velocity of >0.1 m/day. On Negribreen velocities gradually decreases until ≈10 km from the terminus. Down-valley from here, there is not detected any movement, se figure 13. Some lower flow are also seen coming down from Filchnerfonna on the glacier system.

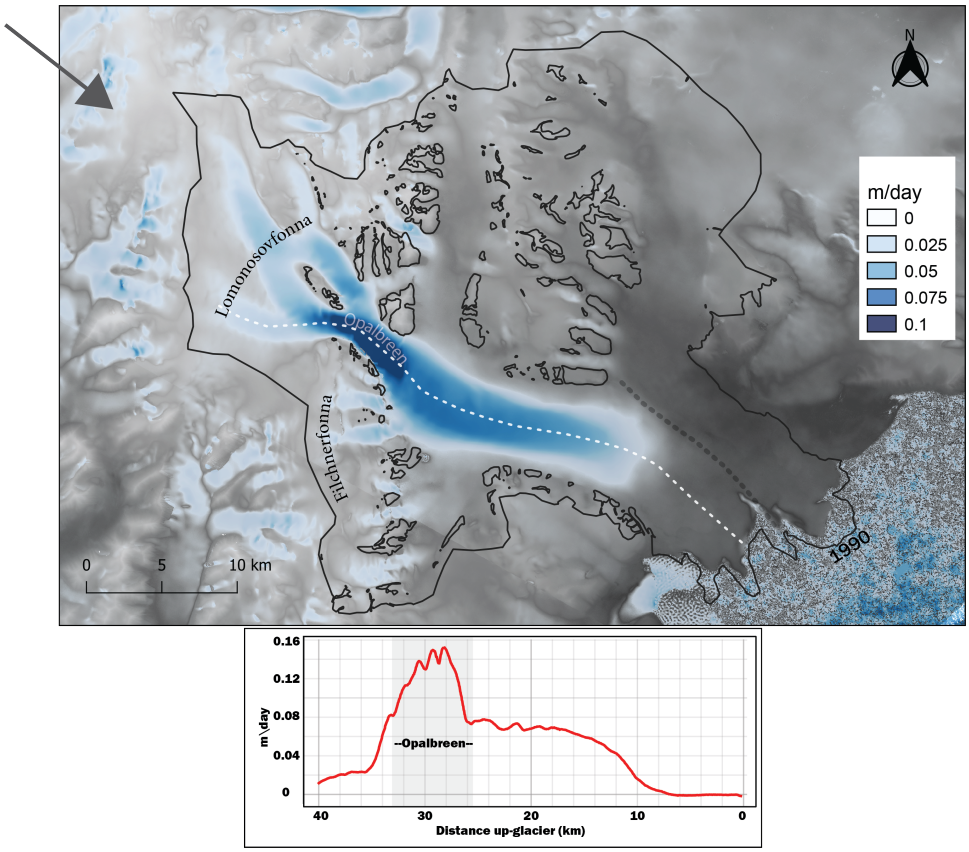

Figure 13: Interferometry velocity map along line of sight (arrow) to the ERS Tandem back in 1995 over Negribreen's glacier system. Signs of higher velocites are seen coming down from Lomonosovfonna. No detection on the frontal zone on the glacier. Profile is from white line.

In 2014 during melt-season, figure 15 show that there are minimal movement over the entire glacier. Along the centerline (see figure 16 A) values are < 0.2 m/d and slightly decelerating down-valley, but the last 2 km towards the coast have a small increase up to ≈ 0.2 m/d. Velocities from June 2015 has only coverage on the glacier frontal zone, but since 2014 there is a increase to ≈ 0.4 m/d at this area. Later in September a distinct development in velocities occurs with speeds increasing to over >1.5 m/d. Throughout autumn/winter 2015 no deceleration is detected at the front, as seen in the December month (figure 16 A). In general, most observed changes in 2014-2015 are limited to the lower 6 km of the glacier.

Approaching spring 2016, velocities low on the glacier have continued to evolve. Noticeably, evolution is limited to an area approximately 2-3 km wide along the first 4-6 km from the glacier front. This is clearly shown during March and April in figures 15 and 16 B, where ice surface velocities increased from 2 to ≈4 m/day, while little/no movement is observed higher on the glacier. Shortly after the melt-season, a steep acceleration takes place as shown in figure 14 (after approximately Julian Day 218-228). This rapid modification in glacier behavior is sustained through the rest of 2016 and towards March 2017 with acceleration evolving over the entire longitudinal surface to the Negribreen. The neighbouring glaciers Akademikarbreen and Rembebreen close to the valley sides show substantial less speed changes.

From 2017 March-June (Julian Day 64-188 figure 14), maximum velocities are around 14-16 m/d throughout the period and acceleration have ceased considerable. This behavior is shown in figure 16, where centerline velocities in March, May and June all have similar values. Later in the melt-season around July, velocities accelerate again. This is a short lived speed peak affecting the whole glacier profile (at least the first 14 km) that lasts less than one month. A high temporal resolution measurement of 5 days with Sentinel-2 image pairs recored 22 m/d at the front which is the highest velocity detected in this analysis (between days 203-208). Shortly after as the melt-season ends, a decelerates occurs towards ≈ 10 m/d at the end of our observations in December 2018 and deceleration rates are sudden throughout. However, as speeds decline on Negribreen, velocities gradually increase close to the glacier edges over the neighbouring glaciers Akademikarbreen and

Rembebreen. This trend is seen when comparing summer 2017 and 2018 velocities in One example of this figure 16 E.

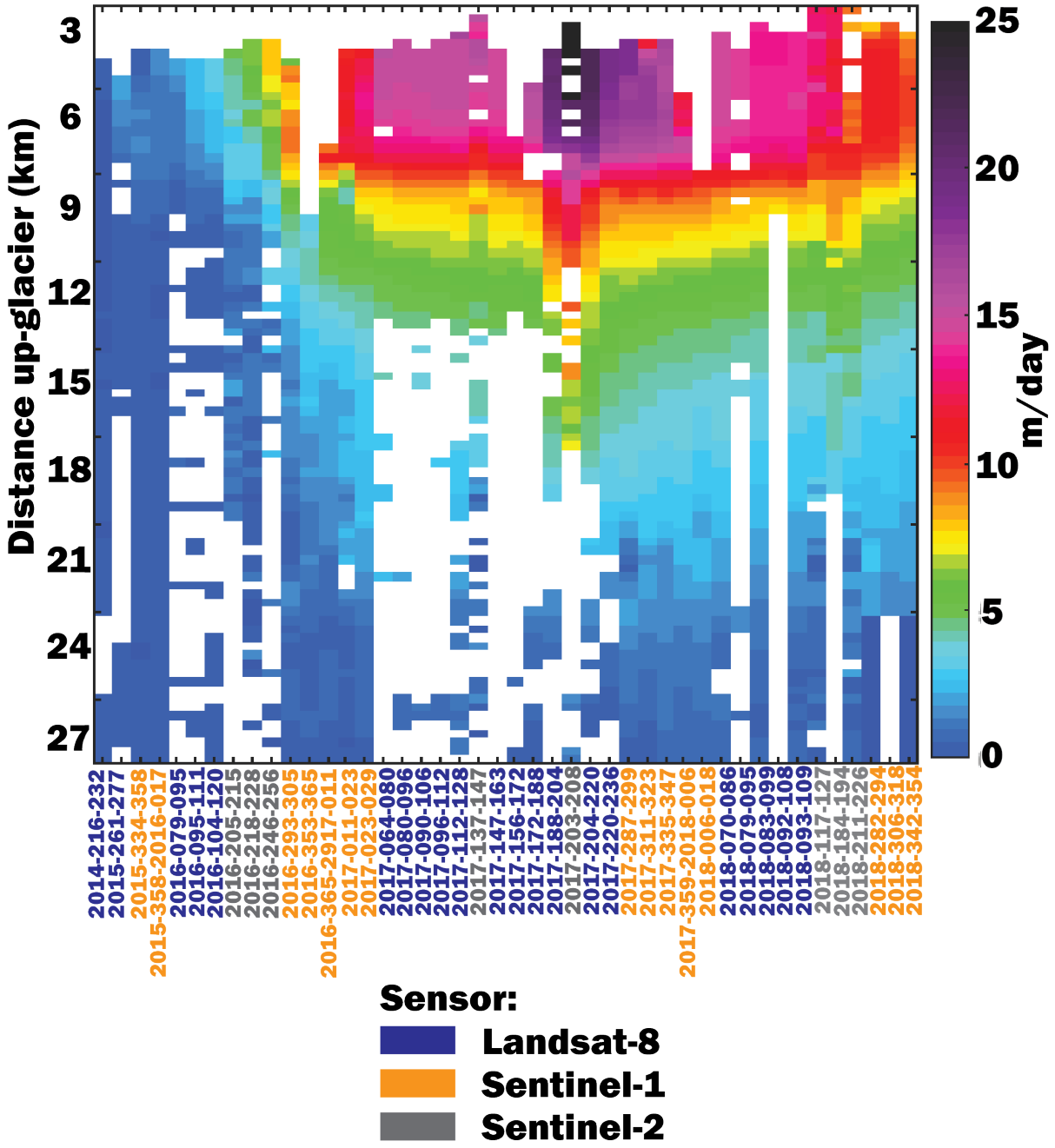

Figure 14: All velocity data from Negribreen presented in m/day along a timeline where the x-axis display dates from 2014 (left) to 2018 (right), in Julian Days. The y-axis shows distance along the glacier centerline (centerline location, figure 6). Each pixel has a seperation of 300 m. Note that velocities from Landsat-8 (blue) has a consistent temporal resolution of 16 day, whereas Sentinel-1 (orange) and 2 (gray) have varying resolutions.

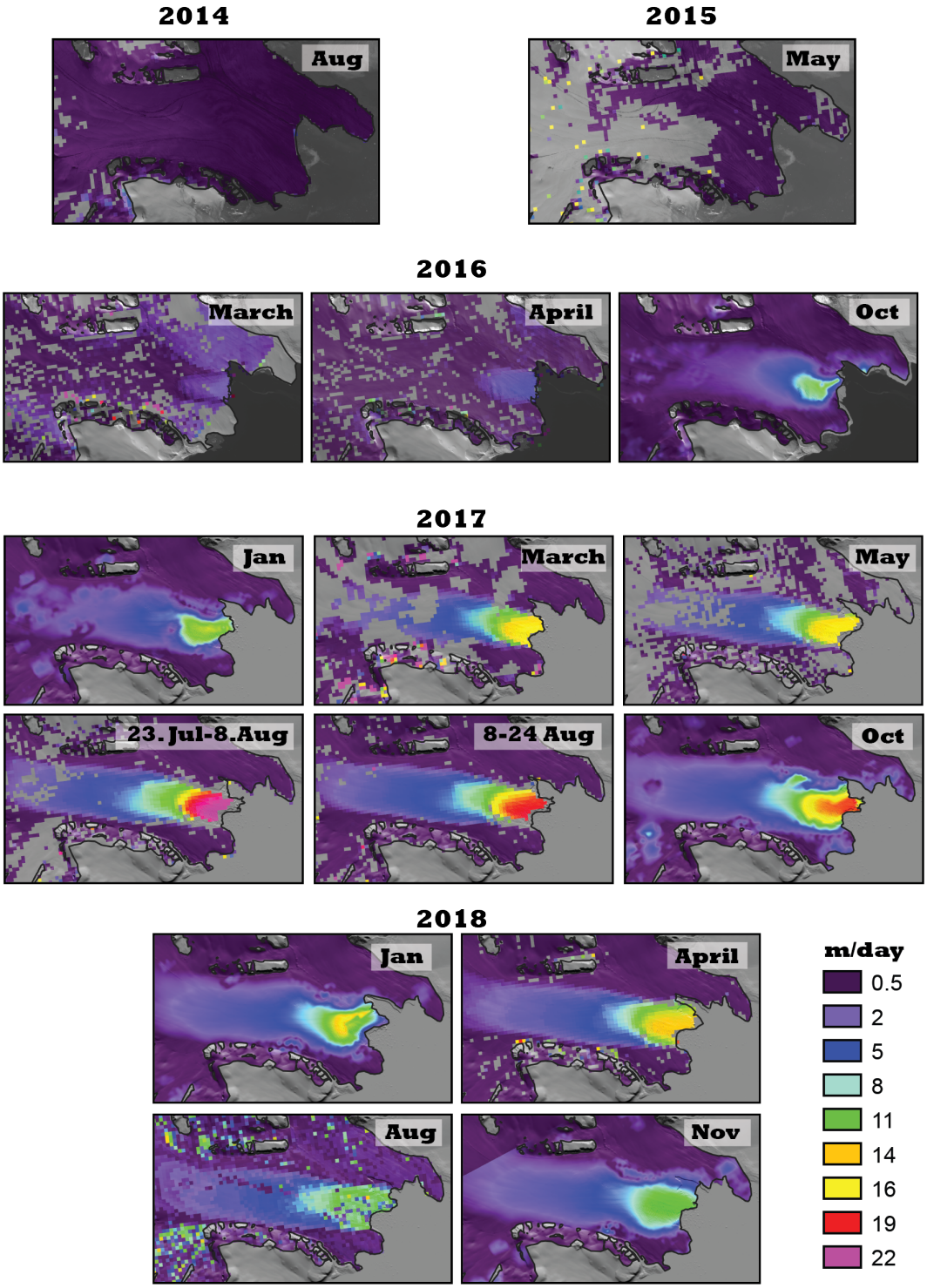

Figure 15: Velocity maps over Negribreen showing important changes in velocity appearances from 2014 to 2018.

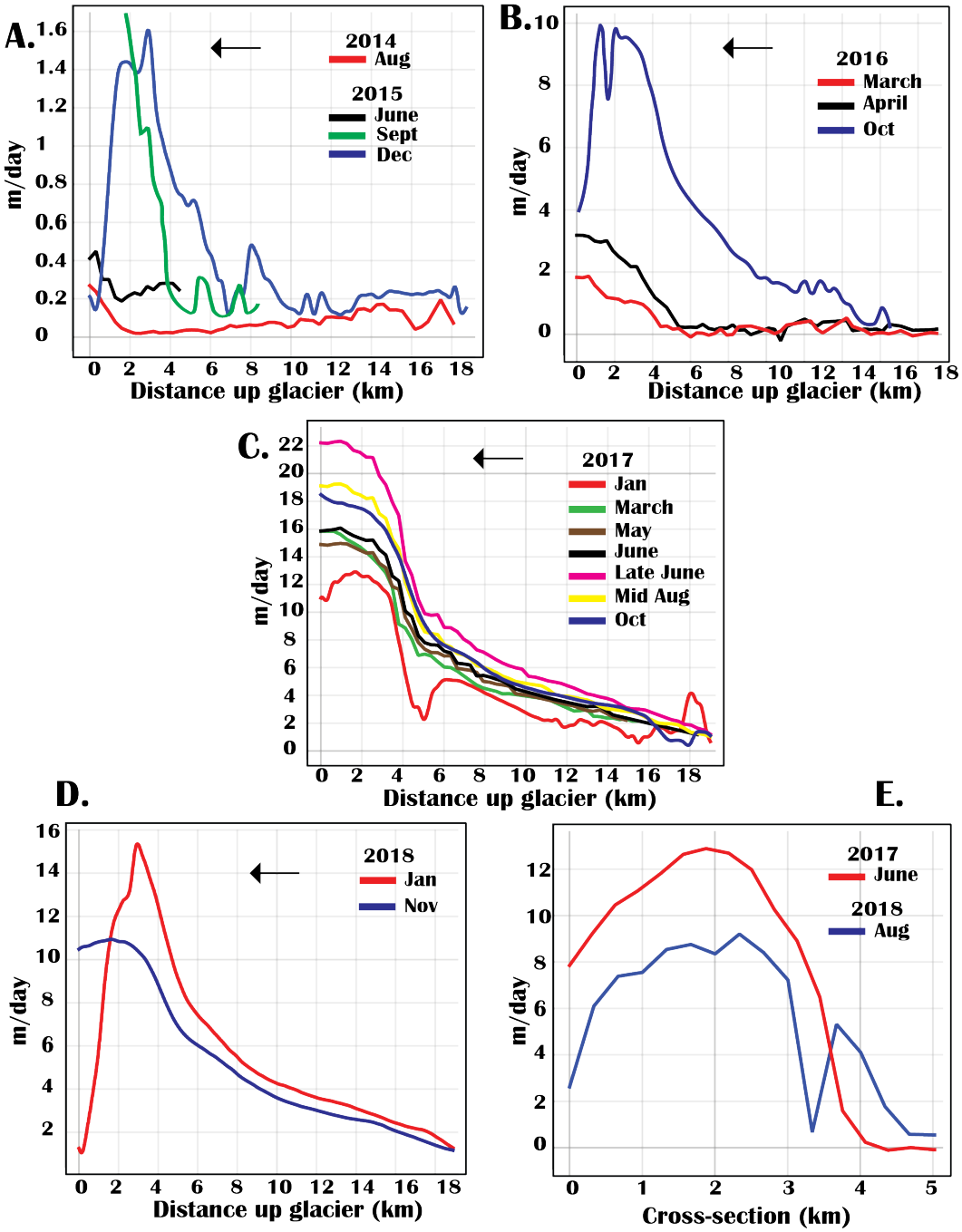

Figure 16: Interpolated velocity profiles over centerline on Negribreen A-D (centerline location, figure 6) showing important steps in velocity appearances. A. Changes in 2004 and 2015. Note the acceleration between June-Sept 2015. B. 2016, where a significant velocity increase occurs over the summer. C. Velocities in 2017. This shows acceleration towards summer and deceleration towards winter. D. Showing a gradual deceleration throughout 2018 and E. A cross-sectional velocity profile over Negribreen and its neighbouring glacier Rembebreen from 2017 and 2018. This shows that velocities are spreading over the glacier surface at the same time deceleration occurs on Negribreen. The negative anomaly between 3-4 km is noise

6.2 Front positions

Overall, the outlines to Negribreen's glacier front clearly show an ongoing retreat at least since 1969 (figure 17 A). By applying the box-method and calculating the ice front's rate of retreat within intervals presented in figure 17 C, we gathered further information about that observation. The findings suggest variations in retreat rates between Negribreen and Ordonnansbreen and Negribreen, which will be referred to as Box 1 and 2 in further text, respectively. In the earliest intervals, outlines in Box 2 retreated at higher rates with 214 m/yr between 1969-1979 and 202 m/yr 1979-1990, opposed to Box 2 which experienced 190 m/yr in both intervals. This reversed within subsequent future intervals, and box 1 give higher retreat values. In 1990-2004 it gives a value of 208 m/yr while box 2 show 164 m/yr. This trend continues and the difference between Box.1 and 2 increases in 2004-2010 with 218 m/yr (Box 1.) and 159 m/yr (Box 2.) and also in 2010-2015 with 276 m/yr (box 1.) and 214 m/yr (box 2.).

The Negribreen front position was analyzed with a higher temporal resolution including every June and December between 2016 and 2018. All measurements are with high resolution imagery from Sentinel-1 and 2 (10 m resolution) which minimizes errors when comparing intervals within this period. During this time period, front positions experienced seasonal variability (figure 17 B. and D.). From June to December 2016 the terminus retreated 649 m. Similarly, large retreats was experienced between the intervals June-December 2017 (730 m) and 2018 (466 m). It thus show that the front retreats as the season shifts from summer to winter. The opposite occurs from winter to summer, when the glacier front advances. From December to June in 2016/2017 and 2017/2018 the ice front advanced 836 and 1126 m, respectively. Moreover, the change of rate on the North and South portion of the front is significantly disproportional, where higher fluctuations occur in the North. The most compelling example of this is between December 2016 and June 2017, where difference in front position becomes less towards the South side of box 3, but very large on the North side.

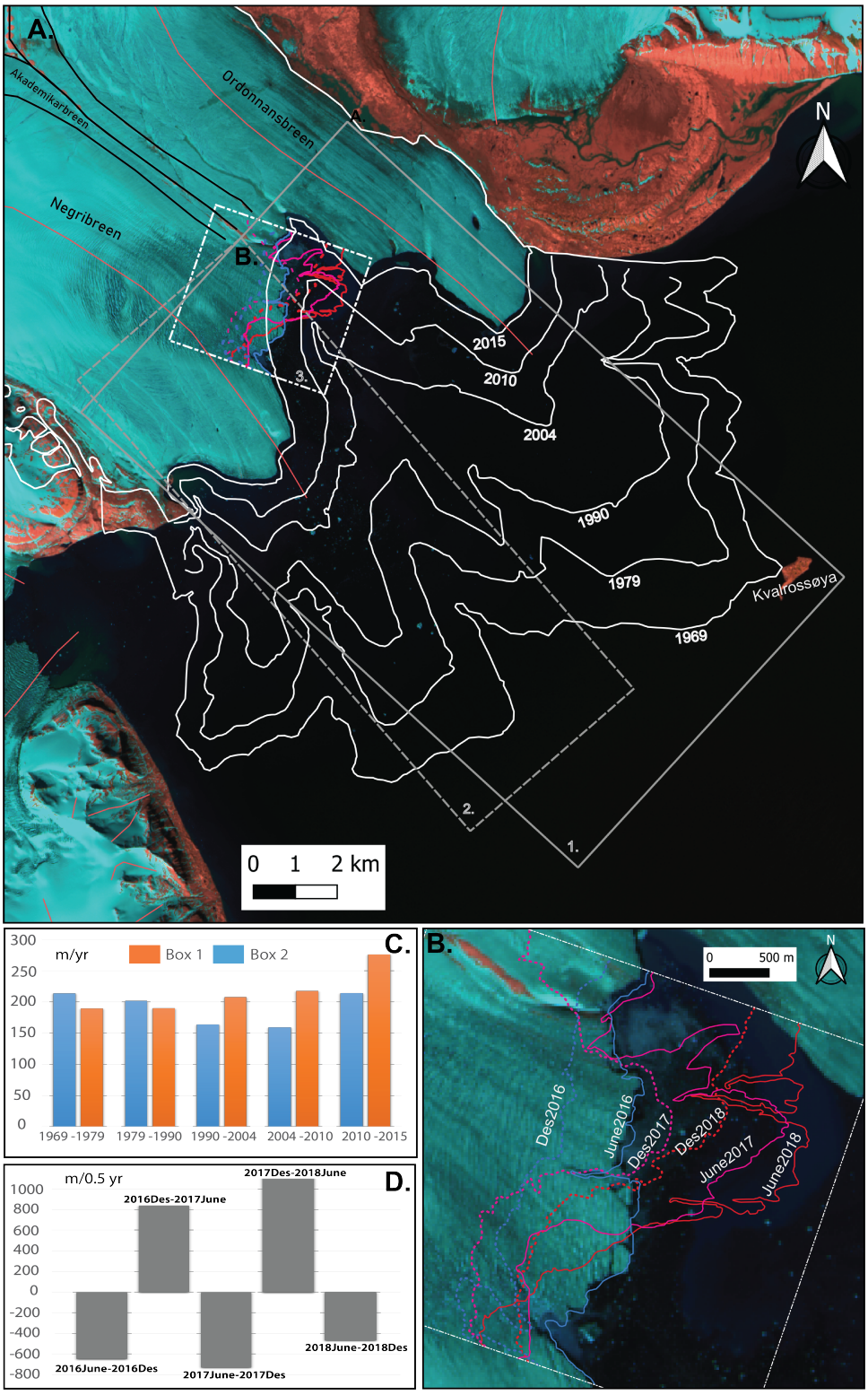

Figure 17: Changes in front position on Negribreen from the Box method since A. 1969 to 2015 and B. Every June and December between 2016 to 2018

6.3 Elevation

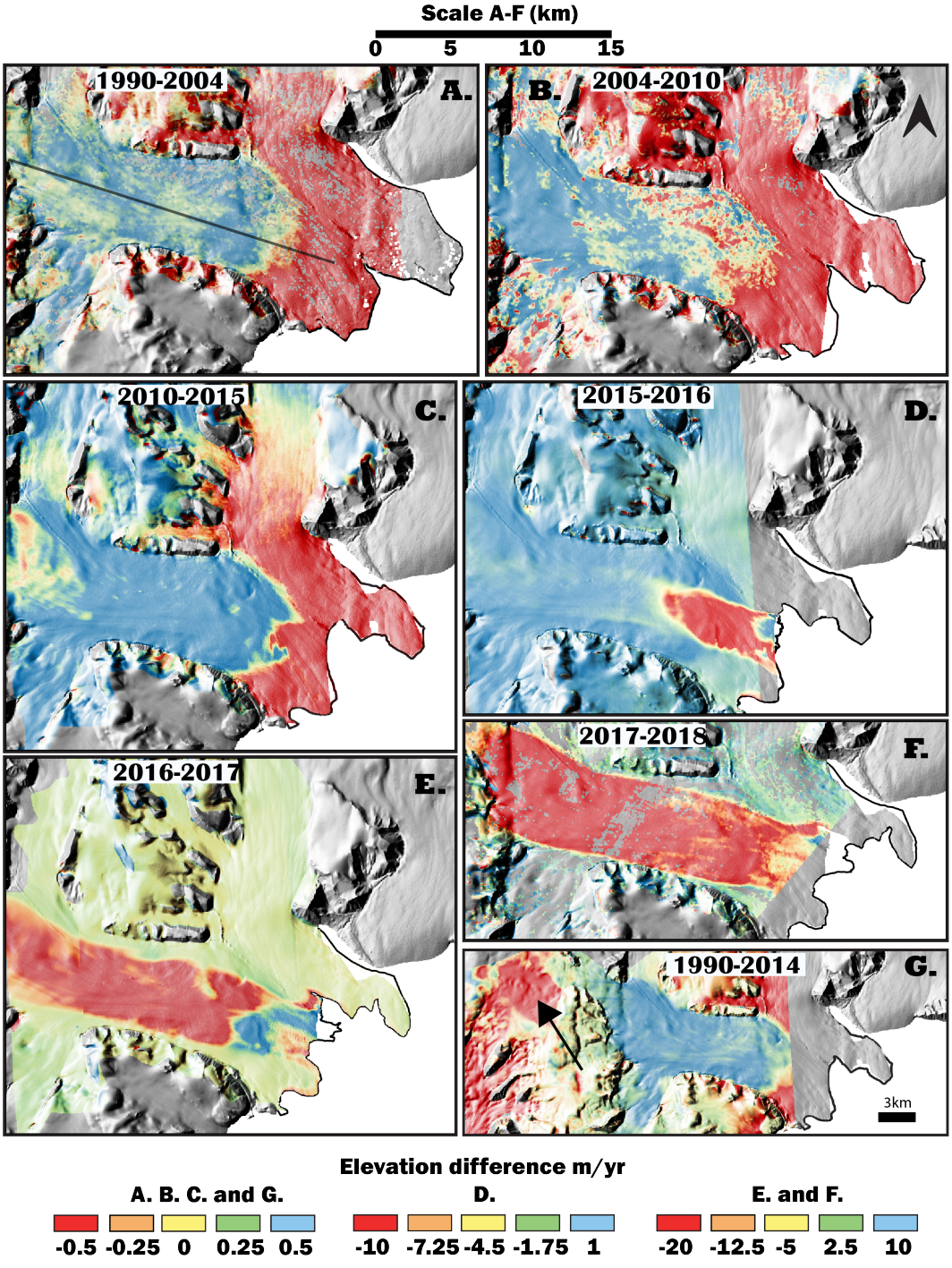

Figure 18: Elevation difference maps presented in m/yr within seven intervals between 1990 and 2018. These intervals show consistent surface thinning and thickening between 1990-2010. The more recent intervals show an accelerating up-propagating surface thinning. A distinct area of affected by surface lowering occur between 1990-2014 (arrow). The line in figure A. are the centerline used for the profiles in figure 19, 20 and 23. The underling base-maps consist of a Tandem-X hill shade from 2011

Over decades, Negribreen shows characterization of a consistent surface lowering on an area low on the glacier, and surface thickening further up-glacier (figure 18 and 19). The lowering is seen in all sub-periods analyzed: 1969-1990, 1990-2004, 2004-2010 and 2010-2015 (figure 19). This effect is most significant closer to the glacier front. In 1969-1990 and 1990-2004 there is a section between 1 and 6 km where thinning rates are fairly similar, where they thin closely around - 1 m/yr. In 2004-2010, the thinning rates shows some higher values around 5 km from the front with ≈ -2 m/yr. A significant increase occurs between 2010-2015 where the rate is much higher than before. Here the elevation lowers with -10/-8 m/yr near the terminus, and the thinning have evolved further up-glacier (18 C). Elevation profiles in figure 20 show that the constant thinning are consequently steepening the surface areas low on the glacier.

Up-glacier from the consistent lowering, the surface has increased in elevation since 1990-2015. Note, the 1969 DEM did not cover this portion of the glacier. In both 1990-2004 and 2004-2010 periods, elevation increases with a more or less similar rate ranging from 0.1 to 0.5 m/yr. From 20 km up-glacier 2004-2010 has some higher rates. Elevation increase more drastically between 2010-2015 around 8-20 km from the glacier terminus, where surface elevates closer to + 1 m/yr. Higher up-glacier the rate decreases similarly to what was seen in 1990-2004.

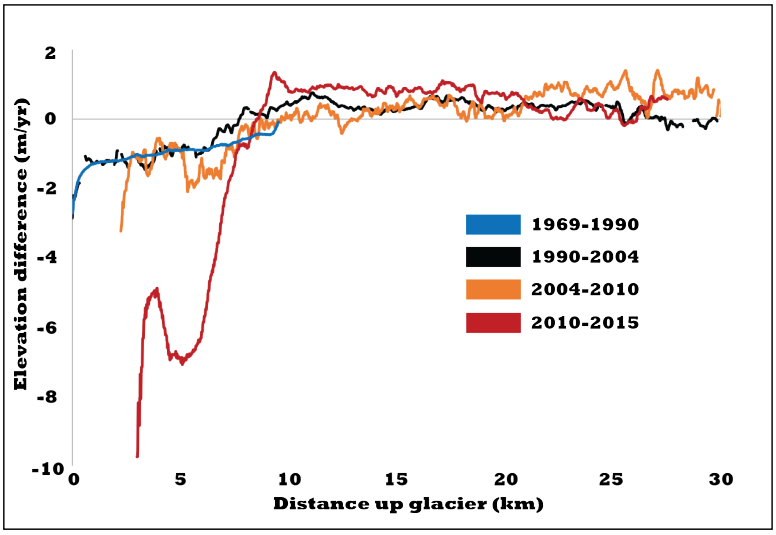

Figure 19: Rate of elevation change in m/yr along the centerline between intervals 1969-1990, 1990-2004, 2004-1010 and 2010-2015

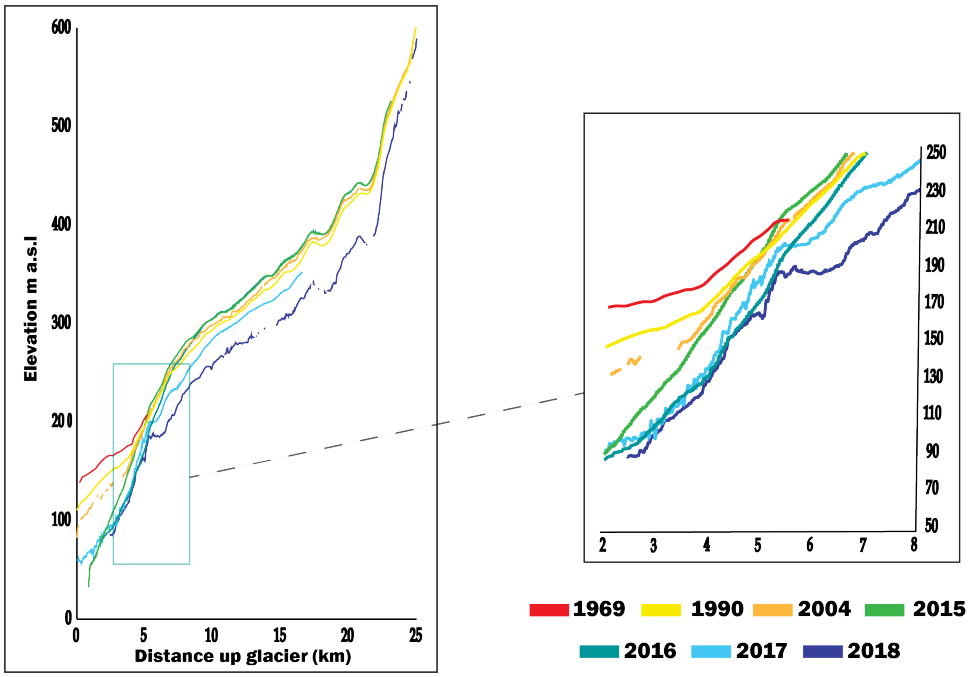

Figure 20: Centerline elevation profiles over Negribreen showing evolution in surface elevation.

Figure 21 shows the intersection lines between surface areas affected by thinning and thickening (at Δ 0 m/yr) from figure 18. This shows that the surface have occurred on relatively stable positions low on the glacier. The figure also includes a small portion of the intersection line from the 1969-1990 DEM differencing (1969 DEM coverage was only on the glacier tongue), and it lies in a similar place to the 1990-2004 and 2004-2010 periods. In 2004-2010 the front is more diffuse on the south portion of the glacier.

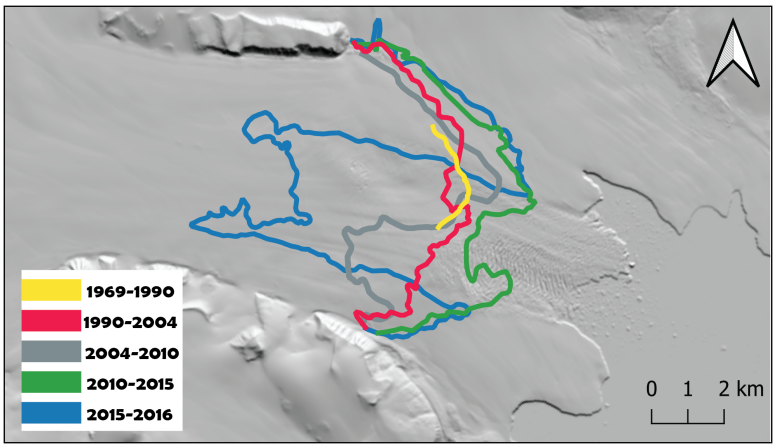

Figure 21: Outlines of the 0 m elevation differences in intervals between 1969-2016. Note that the consistencies in the earlier delineations.

Between 1990 and 2014, DEM differencing detects an evident area of surface lowering on the reservoir zone above Negribreen (arrow in figure 18 G). This area covers a surface of 27 km^2 located south on Lomonosovfonna and show significant thinning rates with a mean rate of -1.4 m/yr (figure 22).

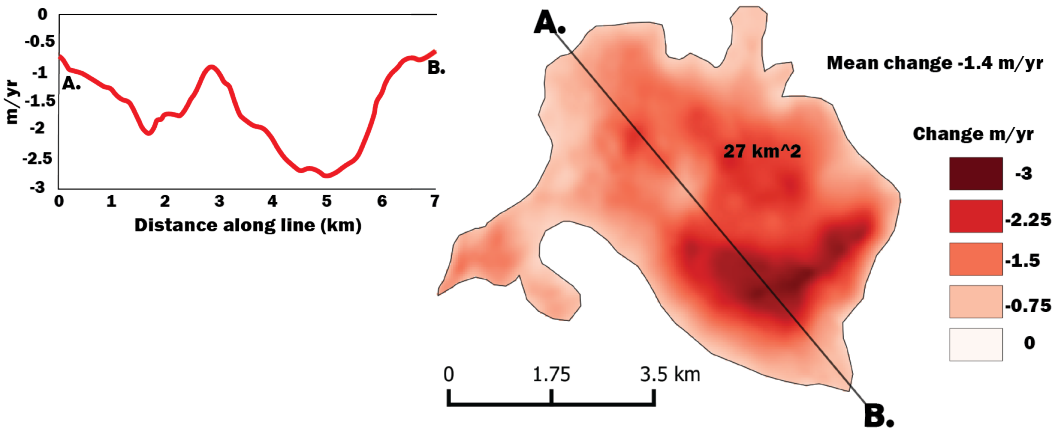

Figure 22: Area affected with a high thinning rate (m/yr) from 1990-2014 on the south portion of Lomonosovfonna (figure 18 G. for location)

In only one year, between 2015-2016, the front portion of the glacier experienced a significant increase in surface thinning. This occur especially between the first 3-10 km from the glacier front as this area show a lowering down to -25 m (figure 23). When comparing elevation profiles from 2015 and 2016, we can see that this has resulted in a rapid thinning of the frontal zone (figure 20. The areas affected by surface thinning have also propagated ≈4-6 km further up-glacier, compared to elevation differencing between 2010-2015 (figure 21). A further modification of the glacier surface occur over the next two successive years (figure 18). Within 2016 and 2017 the whole longitudinal surface of the glacier change. This includes a dramatic lowering of the zone which had a consistent thickening since 1990-2004, where it lowered 20 to 30 m. Low on the frontal zone, the surface have evolved some distinct areas that thickens, with values up to 15 m (figure 23). Over 2017 and 2018, further rapid lowering have modified the surface. In figure 20, we see that the thinning has especially affected the glacier surface after 5 km up-glacier. It is noteworthy that these modifications initiates centered on Negribreen, and gradually spreads towards the valley sides (figure 18 D, E and F).

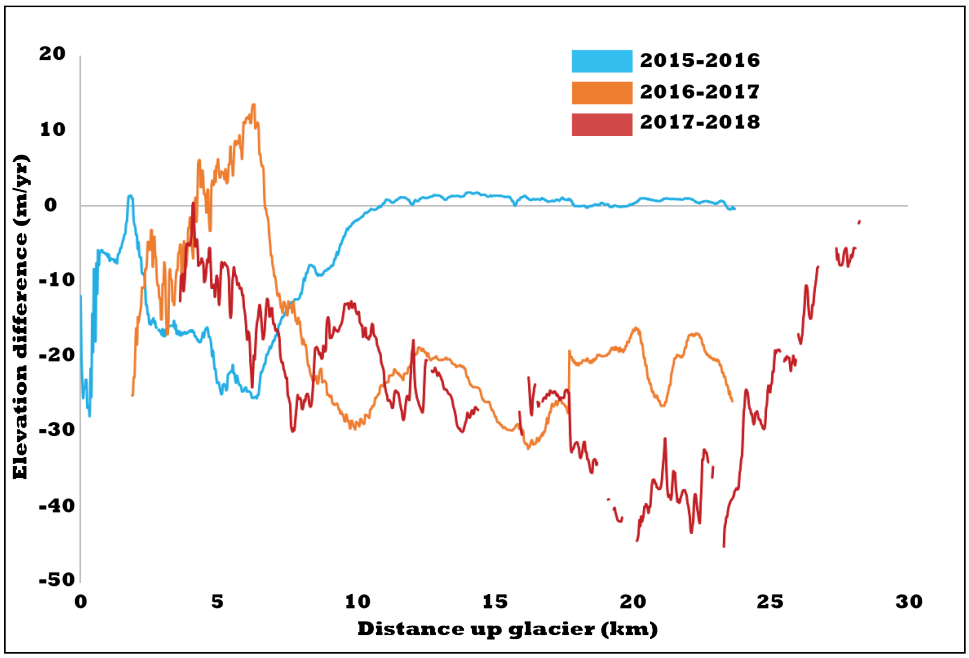

Figure 23: Rate of elevation in m/yr change along the centerline during 2015-2016, 2016-2017 and 2017-2018

6.4 Surface structures and sea-ice

Several obvious changes on the ice surface take place after 2015 (figure 24). In August 2015 the whole glacier appears relatively smooth with the exception of the very edge of the glacier front, where some small fracturing is detected (figure 24 A). Figure 24 B shows a larger portion of the front being influenced by fracturing one year later. Here a distinct crevasse-field has evolved, covering an area of $\approx$ 10 km^2. By August 2017 this covers almost the entire glacier and is most deformed closer to the terminus. Surfaces on the sides such as Akademikarbreen show less deformation, and especially on Negribreen's South portion towards Rembebreen. The crevasses are noticeably intensified in August 2018 and they have migrated closer to the side as well (figure 24 C and D). The crevasses are mostly longitudinal and perpendicular to flow. There are also evolving medial loop moraines, shown in figure 24 B1,C1 and D1.

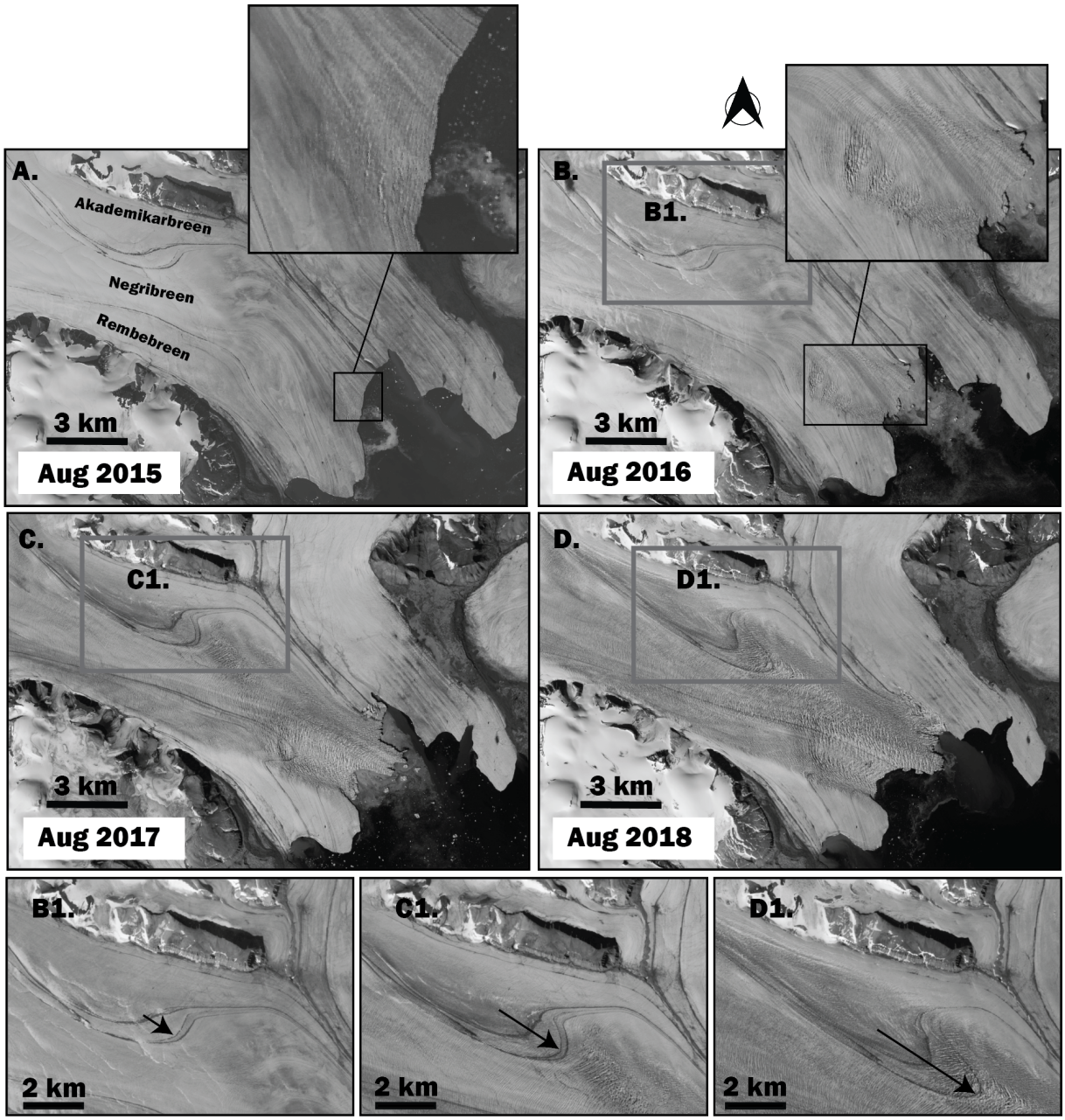

Figure 24: Surface structural changes on the bottom half at Negribreen with a one year interval from 2015-2018. A. Landsat-8 panchromatic band image. No crevasses except a small area near the terminus. B. Distinct crevasse field on the glacier tongue. C. Crevasses evolving up glacier. D. More heavy crevasses than 2017 B1,C1, D1 evolving medial looped moraing 2016-2018

7 Interpetation and discussion

7.1 Pre-collapse: development of bulge

Observations show a bulge on the lower portion of Negribreen. The persistent surface lowering at the frontal zone and the thickening further up-glacier indicate a development over a long time, possibly stretching over 25 years (figure 19 and 20). Interferometry from 1995 suggests that ice is being transferred from the Lomonosovfonna reservoir to the lower regions of Negribreen. This is most likely a main source for the elevation thickening 10-20 km from the glacier terminus (see figure 13). Interestingly, the velocity snapshot reveals no detectable movement on the frontal zone where there is constant surface thinning. This suggest high basal friction and is an important factor for the bulge development. The zone of high friction may act like a barrier for the mobile ice coming down, forcing it to "pile up". As shown in figure 21, the intersection line of where ice surface is thinning and thickening is located fairly consistently low on the glacier since 1969. This may indicate long-term stable basal friction on the lower section of Negribreen.

Conditions with high friction are highly related to the glacier thermal regime, where ice below the pressure-melting point freezes to its bed (Nuth et al., 2019; Kääb et al., 2018). However, it was discussed in Sevestre et al. (2015), that influence of the thermal regime on surge-type glacers varies according to their sizes and whether they terminate on land or in water. In this study airborne ground penetration radar (GPR) was conducted on six Svalbard glaciers along their centerlines. Although such GPR investigations may in certain cases only be an indication of the thermal regime, the findings indicated that smaller land terminating glaciers had fully cold thermal regimes, which is probably reflecting the present general inactivity on such glacier on Svalbard. On the larger Von Postbreen and Kongsvegen glaciers, which are deep into their apparent quiescent phase, the GPR showed there is still temperate ice over the bed. However, large terrestrial glaciers such as Von Postbreen and also Bakaninbreen (Hodson et al., 1997), have cold ice on their terminal zones where ice is thin. This was not showing on the tidewater glaciers Tunabreen and Kongsvegen, where there were temperate ice under most of their beds. Furthermore, Dowdeswell et al. (1984b) conducted an air airborne echo sounding survey over parts of Negribreen in spring 1980. From the collected data, variations in the ther-

mal regime along the glaciers longitudinal profile was interpreted, as warm and cold ice influence the echo waves differently. According to the findings at that time, Negribreen had temperate conditions on the lower portions with a overlying layer of cold ice, $\approx$ 20 m thick. Thus these observations contradict with the idea of friction due to large portions of Negribreen are frozen to the bed.

On another tidewater glacier in Svalbard, Nathorstbreen, Nuth et al. (2019) described long-lasting friction on the glacier tongue, using a thermo-mechanical model. It was argued that cold patches at the bed could be sufficient to reduce mean basal sliding. This would then eventually stabilize an efficient drainage system through large channels in the sediments (if a sufficiently thick sediment layer is present) and promote high friction. The cold patches were thought to appear where advection of warm ice is minimized, such as under medial moraines. This theory is interesting because from multibeam swath-bathymetry just outside Negribreen's modern terminus, Ottesen et al. (2017b) detected eskers on the sea-floor. Eskers are deposits formed from long-term stable efficient drainage systems out of the glacier (Dowdeswell and Ottesen, 2016). This is indicative of a an efficient drainage systems having been present under Negribreen, and thus shows some interesting parallels with Nathorstbreen. If large channels are submerged in a sufficiently thick sediment layer beneath Negribreen and able to deliver high flow capacity over time, it could ensure low basal pressure and possibly allow the tongue to sustain in a high friction state.

7.2 Pre-collapse: surface dynamic Initiation

Distinct signs imply Negribreen was undergoing a dynamic transition towards 2015. Between 2010 and 2015 there is a higher rate in elevation lowering which also starts propagating up-glacier from the bulge-front (figure 19 and 18 C). There is also a jump in velocities seen from $\approx$0.2 m/day in August 2014 (figure 16) to >1.5 m/day (figure 16) in September 2015 at the glacier front. This velocity increase could also suggest that rapid thinning between 2010-2015 (figure 19) occurred closer to 2015 as there seems to be a clear relationship between surface lowering and increased ice surface movement. However, most velocity increase occurs between June and September 2015 where a change from $\approx$0.4 to

≈1.5 m/d is detected (see figure 16). Towards December 2015, there is minimal velocity deceleration occurring at the glacier front and there is even minor velocity increase 2 km further up-valley (figure 16). This is the opposite of what would be considered in a non-surging glacier, where velocities tend to decrease from summer to winter. The lack of a winter reduction of velocity could suggests that a fundamental change in glacier dynamics is occurring.

These dynamic behaviors strongly imply a process that triggers a reduction in basal friction on the glacier frontal zone. This possible includes basal melt water production from increased driving stresses, a direct result of the surface thinning and steepening. As explained in equation (1), driving stress is calculated from ice density, gravity, thickness and surface slope, and increases in both driving stress and strain rate will eventually cause melting of the ice at and above the bed, which promotes glacier movement (Van der Veen, 2013). As elevation differences from 2010-2015 show (figure 19), thinning rates on the frontal zone are significantly larger than what thickens further up-glacier. Combined with a continual glacier retreat this is reflected as a thinner and steeper surface slope in 2015 (figure 20). Consequently the steepening on Negribreen would increase driving stresses at the same time thinning of the surface would decrease possible thresholds. This would then cause higher melt rates. The disproportional thinning/thickening ratio during 2010/2015 is compelling when comparing to any of the earlier periods in figure 19. Similar arguments have been made on other tidewater glacier such as Fridtjovbreen and Aavatsmarkbreen (Murray et al., 2012; Sevestre et al., 2018). On Aavatsmarkbreen, Sevestre et al. (2018) observed a thinning gradient low on the glacier that doubled between 1990 and 2010 while mean thickness increased with only 24 % , and was argued for producing basal melt and acting as a trigger for instabilities. On Fridtjovbreen, Murray et al. (2012) also concluded that a thinning and steepening of the surface slope triggers instabilities, but further argued that this effect doesn't need to be in a combination with a surface thickening.

Acting as an external factor, sea ice concentrations have a significant influence on a tidewater glacier via their control on calving rates (Carr et al., 2014). The role of sea ice on glaciers have particularly been investigated on Greenland. For instance, on Jack-

obshavn Isbrae, Joughin et al. (2008) showed that seasonal influences of sea-ice occur depending on the timing of its onset towards winter and break-up towards spring. Where sea ice evolves early, ice-mélange was prevented from leaving the fjord, and the longer sea ice are present towards spring, calving is suppressed. Similar effects was shown on several glacier on the Novaya Zemlya island, inn in the Russian Arctic (Carr et al., 2014). In the fjord where Negribreen terminates, snapshots from Landsat-8 imagery show substantial earlier sea ice break-up in 2014 and especially in 2016, when compared to 2013, 2017 and 2018 (figure 25). This indicate favorable conditions so that internally driven factors could more effectively destabilize the glaciers frontal zone. However, to draw conclusions about the impact of sea ice on Negribreen, a more in depth analysis is needed.

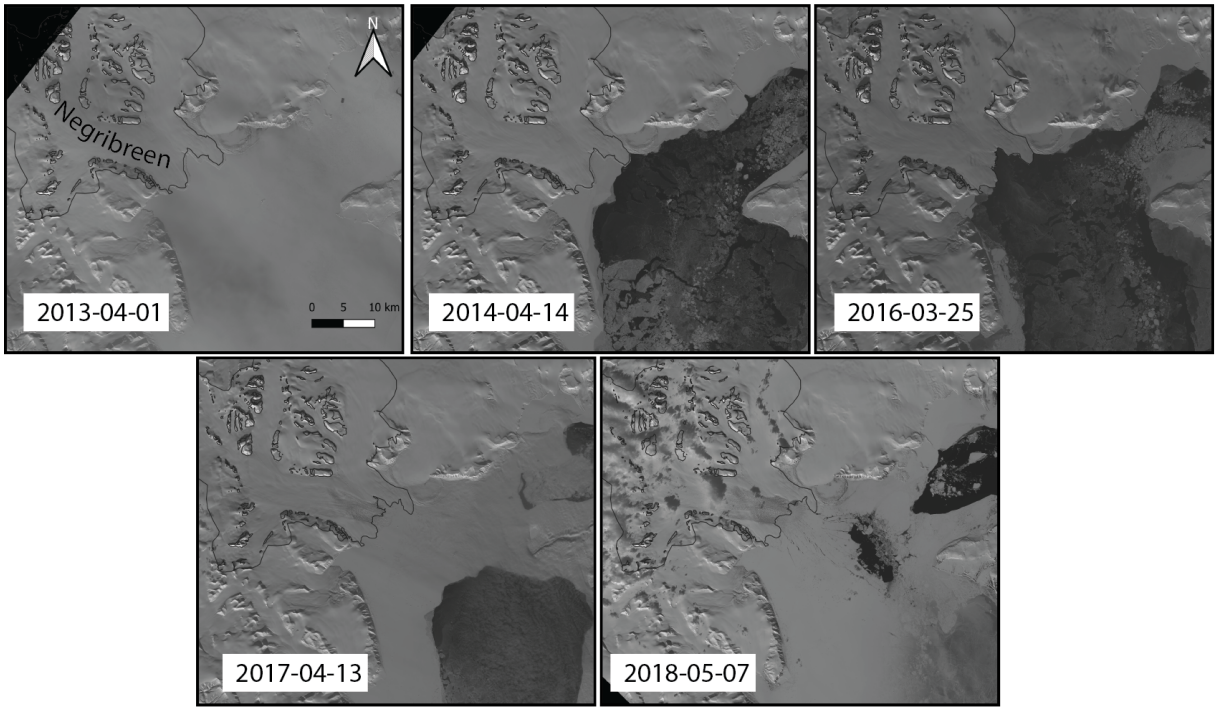

Figure 25: Sea-ice coverage over the cost outside Negribreen in 2013, 2014, 2016, 2017 and 2018 from Landsat-8 panchromatic band. No image from 2015 due to clouds

7.3 Collapse

Approaching spring 2016, changes in horizontal velocity were most widespread on the glacier tongue and fade out quickly further up-glacier. For instance in March/April, velocities rise from 2 to almost 4 m/day within 2-3 weeks, while further up the ice remains more static (figure 16). Higher movement is restricted to where there is a crevasse field

on the tongue, which has become more intensified and covers a substantially larger area than in summer 2015 (figure 24). The crevasses are predominantly perpendicular to flow, indicative of extension, which also explains the larger thinning rate of up to 25 m/yr occurring between summer 2015/2016 (figure 18D and 23).

In late summer 2016, it seems like basal shear stresses finally overcame an internal threshold which triggered a collapse of the high friction zone. Although there are no direct observations of a till layer or its properties under Negribreen, the DEM differencing between 2015 and 2016 in figure 23 suggests that there is such a layer. In this interval, the glacier surface thins rapidly only down-glacier from the friction zone transition, before the 10 km mark which could resemble a failure in till. Fowler et al. (2001) presented a model of thermally regulated surges over soft beds. The critical parameters in this model are the thickness and permeability of unfrozen till, and these properties determine the rate of the active surge onset. Prior studies have supported a thermally regulated soft bed surge mechanisms on Svalbard surge glaciers, such as field observations of polythermal regimes from Murray et al. (2000) and statistical studies from Hamilton and Dowdeswell (1996) and Jiskoot et al. (1998) that have shown polythermal glaciers tend to overly sedimentary bedrock. This means that the collapse may occur from a elevated pore pressure which caused a failure in the underlying till.

As a response to the collapse, high ice surfaces velocities are no longer restricted to the frontal zone. An activation wave of significant velocity acceleration propagates both up and down the glacier (figure 16 and 15). The precise timing of the collapse is thought to be at the summer/autumn changeover in 2016. This is just before a rapid velocity acceleration that affected almost the whole longitudinal part of the glacier with within a few months. The transition is shown in figure 14; at kilometer 0 to 5, velocities climb from $\approx$5 to $\geq$10 m/day, at kilometer 5 to 10 they rise from $\approx$0.5-2 to 5-7 m/day and from kilometer 10 to 15 they increase >1 to $\approx$3 m/day (measured up-glacier). The timing of collapse seems consistent when comparing to observations presented by Nuth et al. (2019), where increased seismic events from Negribreen were detected from the SPITS array in Longyearbyen (measuring glacier related ice-quake activity such as calving) during this time.

Effect of surface-melt input

Post-collapse, figure 14 show that rapid expansion of high velocities discontinued after March 2017. Through the next months until early June, there were relatively constant speeds (figure 16). This seems to be controlled by melt-water or the ability to modify the drainage system, as shortly after this, in July 2017 (Julian Day 203-208), a short-lived velocity peak occurred. Speeds reached >22 m/day at the front and increasd rapidly over the entire glacier profile. At this point crevasses have evolved to cover almost all surface area on Negribreen.

After the initiation of glacier dynamics in 2014, melt seasons have been an important contributing factor for causing further dynamics response, which is directly reflected in the increasing velocities, surface thinning and crevasse patterns. Velocity increase promotes a larger crevasse field from each successive summer. This provides an additional source of melt-water lubricating the bed, which leads to more deformation, thus forming a cycle of positive feedback. Observation from Schellenberger et al. (2014) also showed that the variability in glacier speed on Kronebreen and Kongsvegen correlated with variations in amount and timing of surface melt water input to the bed. Furthermore, the evolution of crevasse patterns on Negribreen is very similar to what is seen at other comparable glaciers such as Tunabreen, Comfortlessbreen, Aavatsmarkbreen and Wahlenbergbreen, among others (Flink et al., 2015; King et al., 2016; Sevestre et al., 2018). Similarly to Negribreen, crevasses on all these glaciers initiate at the terminus and migrate further up-glacier and showed strong correlation with surface speeds.

Additional melt-water input further affects the thermal structure of the glacier, a term called cryo-hydrological warming (CHW) that includes latent heat released during refreezing of meltwater and direct heat transfer between water and ice (Phillips et al., 2010). CHW has the potential to change englacial and basal temperatures within years, whereas changes in basal thermal regime by heat production alone would require decades to centuries (Phillips et al., 2010). This effect enhances itself especially in melt-seasons; during the crucial seasons before Negribreen's collapse there were evident "step-increases" in velocities over two successive summers in 2015 and 2016, where the melt produced in

2016 allowed the basal conditions to exceed some thersholds which let to collapse. Also in 2017 velocities increased a lot in the melt season after several months with stagnant movement. This pattern was nicely documented by Dunse et al. (2015), who observed that the multi-annual acceleration during surge initiation on Basin-3, Svalbard, was occurring in steps, coincident with successive summers. It was argued that hydro-thermodynamic feedback triggered the final surge as surface melt was reaching a growing fraction of the glacier bed. It seems that after the first initiation of instabilities through basal stresses there rapidly become imbalances in the glaciers enthalpy. Enthalpy is a measure of the internal energy of a glacier containing informations about the ice temperature and water content (Aschwanden et al., 2012).

The positive feedback in dynamics that increased melt water has on Negribreen implies that ice near the edges of the glacier are fully/partially frozen to their beds. This is suggested as these areas display both lower velocities and fewer crevasses (figure 16 and 24). As more melt water occurs at the bed, either produced by basal shear stresses or surface melt, the static sides act like a blockade on it, promoting an inefficient drainage system.

7.4 Post-Collapse: deceleration

Shortly after the velocity peak in July 2017, Negribreen underwent a steady deceleration along its entire longitudinal profile. As far temporal coverage in this analysis show (see figure 14), this deceleration began near the end of July 2017 (Julian Day 203-208) and continued to December 2018 (Julian Day 342-354). Towards the end of 2018, velocities were still fairly high, $\approx$ 10 m/day. It seems probable that deceleration will continue over the next several seasons, and could last longer than the acceleration phase. In summer 2018 crevasse zones have become considerably more extensive on the glacier surface. Presumably this would enable increased surface-to-bed drainage once again. There is little to indicate a seasonal signal in velocities, with the exception of a few minor areas 10-15 km up glacier (see figure 14 Julian Day 184-194). This lack of a "velocity-boost" during melt-season is the first since the 2015 season. This implies establishment of a more persistent efficient drainage system. Figure 15 and 16 show enhanced velocities on both sides to-

wards Akademikarbreen and Rembebreen, and in addition to more evolved crevasses (see figure 24) this suggest at least one extra source of gradual water-leakage from beneath the glacier. The deceleration is also controlled by ice thinning, which in turn is contorlled by the rate of transport of ice downglacier (Murray et al., 2003).

7.5 Seasonal front behavior

After a continues retreat since 1969, Negribreen advances between 2016 and 2018. Not all surges lead to ice front advances (Benn and Evans, 2014), but studies have shown that Svalbard tidewater glaciers tend to advance during their active phase. This was shown on Fjortende Julibreen, Monacobreen, Comfortlessbreen and Blomstrandbreen where it was seen that increased terminus rates closely matched the velocity increase (Mansell et al., 2012). However, the similarities to these glacier stops here, because the mapped front positions between 2016 and 2018 on Negribreen show clear signs of seasonal fluctuations, where the front retreats during June-December and advances December-June (figure 17 D). For instance, the terminus had a mean retreat of $\approx$ 650 m from June 2016 to December, even thought ice flow rapidly increased. This contrast to the findings according to Mansell et al. (2012), that seasonal cycles of the terminus positions diminish during the active phase, and only when the glacier speeds had returned to its pre-surge flow rate the terminus show signs of this.

The seasonal front fluctuations on Negribreen implies behavior similar to a traditional tidewater glacier, as been observed on several glaciers on Greenland (Howat et al., 2010; Schild and Hamilton, 2013) and Alaska (McNabb and Hock, 2014). Although it is too early to say for Negribreen, but the decrease in subglacial friction and the highly evolved crevasse field on the glacier surface, could suggest a result in an prolonged deceleration phase, compared to other glaciers on Svalbard. In a more extreme scenario it could potentially caused a change in the glacier flow regime, towards a long-lasting "typical" tidewater behavior, such like the Svalbard glacier Kronebreen. This tidewater surge-type glacier is the most continues fast flowing glacier in the region, having had constant high seasonal front rates for decades (Sund et al., 2011). In general, glacier advances when flow rates are higher than the ablation, and a glacier retreats when frontal ablation rates exceeds

the glacier flow (Schellenberger et al., 2014). An important process of the frontal ablation on tidewater glaciers is ice berg calving. According to Luckman et al. (2015), the biggest factor showing a link to the seasonal terminus rates on Kronebreen, was changes in the sub-surface ocean temperature (second-order process). This could possible contradict for Negribreen acting like Kronebreen, as Negribreen is located on the east side of Svalbard and are influenced by the colder water of the of the East Spitsbergen Current (ESC) as oppsosed to the warmer West Spitsbergen Current (WSC) which affects Kronebreen. However, primary controls such by stretching of the ice body due to speed gradients and subsequent opening and propagating of crevasses heavily influence ice berg calving as well (Benn et al., 2007). Negribreen has a substantial bigger surface area for crevassing

7.6 Bulge evolution before detection

Data coverage reveals limitations when it comes to understanding the full evolution of the bulge development. It is difficult to say whether it came propagating from the reservoir area, or always developed gradually from a low stagnant position before its detection. DEM-differencing already suggests the development of bulge low on the glacier for several decades, since 1990 and possibly even earlier towards 1969. Thus it is plausible that the bulge was created from ice steadily being drawn down and away from the reservoir and developed where there is a zone of high friction, rather than being pushed through the glacier system. It should be mentioned that this stage of a surge is poorly studied because of difficulties recognizing surges on an early stage (Sund et al., 2009) and due to limiting data coverage. To our knowledge this hasn't been observed before and lacking data in this study makes it difficult to elaborate any further.

8 Conclusion

From remotely sensed techniques, with high temporal resolution data, we investigated the collapse of Negribreen, a tidewater glacier on the east coast of Svalbard. Observations through velocities, elevation changes, glacier extent positions and surface features have highlighted dynamic processes since 1969. From this we present strong arguments that the collapse, in 2016 summer/autumn changeover, is a result of two phases. Phase (1) is long-lasting and characterized with a slow flow regime and a retreating front. Throughout this phase, surface thickening occurs on the upper half of the ablation zone as ice are being transferred from its reservoir area. The lower ablation zone has a persistent surface steepening, which increases driving stresses, and thinning, which consequently lowers potential driving stress thresholds. The bed under the glacier frontal zone is characterized with a zone of high friction throughout the phase. It is unlikely that the subglacial friction is controlled by the thermal regime alone and are proposed to rather be a consequent of the properties in the drainage system. Eventually, these dynamic processes results in enough basal melt to initiate surface dynamics and promotes the second phase. (2) This phase is characterized with an accelerating flow regime, rapid surface lowering, and up propagating crevassing. Effectively this cause a cycle of positive feedbacks through melt water input, which destabilizes the frontal zone until the collapse. Our observations have shown that the key factors in both phases resemble several comparable tidewater glaciers on Svalbard. We have further highlighted through interpretation, that a subglacial till layer have potentially influenced the surge behavior. The true impact of this on Negribreen, and on other surging glaciers on Svalbard, remains as an uncertainty and needs further investigation.

References

Altena, B. and Kääb, A. (2017). Weekly glacier flow estimation from dense satellite time series using adapted optical flow technology. *Frontiers in Earth Science*, 5:53.

Arnaud, E., Halverson, G. P., and Shields-Zhou, G. (2011). *The geological record of Neoproterozoic glaciations*.

Aschwanden, A., Bueler, E., Khroulev, C., and Blatter, H. (2012). An enthalpy formulation for glaciers and ice sheets. *Journal of Glaciology*, 58(209):441–457.

Benn, D. and Evans, D. J. (2014). *Glaciers and Glaciation*. Routledge.

Benn, D. I., Warren, C. R., and Mottram, R. H. (2007). Calving processes and the dynamics of calving glaciers. *Earth-Science Reviews*, 82(3-4):143–179.

Bindschadler, R., Harrison, W. D., Raymond, C. F., and Gantet, C. (1976). Thermal regime of a surge-type glacier. *Journal of Glaciology*, 16(74):251–259.

Blatter, H. and Hutter, K. (1991). Polythermal conditions in Arctic glaciers. *Journal of Glaciology*, 37(126):261–269.

Boon, S. and Sharp, M. (2003). The role of hydrologically-driven ice fracture in drainage system evolution on an Arctic glacier. *Geophysical Research Letters*, 30(18).

Boulton, G. S., Wright, A., and Moseley, F. (1975). Processes and patterns of subglacial sedimentation: a theoretical approach. In *Ice ages: ancient and modern*, volume 6, pages 7–42. Seel House Press Liverpool.

Braun, M., Pohjola, V. A., Pettersson, R., Möller, M., Finkelnburg, R., Falk, U., Scherer, D., and Schneider, C. (2011). Changes of glacier frontal positions of Vestfonna (Nordaustlandet, Svalbard). *Geografiska Annaler: Series A, Physical Geography*, 93(4):301–310.

Brown, L. and Duguay, C. (2011). The fate of lake ice in the North American Arctic. *The Cryosphere*, 5(4):869.

Brown, R., Derksen, C., and Wang, L. (2010). A multi-data set analysis of variability and change in Arctic spring snow cover extent, 1967–2008. *Journal of Geophysical Research: Atmospheres*, 115(D16).

Carr, J. R., Stokes, C. R., and Vieli, A. (2014). Recent retreat of major outlet glaciers on novaya zemlya, russian arctic, influenced by fjord geometry and sea-ice conditions. *Journal of glaciology.*, 60(219):155–170.

Casassa, G., Espizua, L., Francou, B., Ribstein, P., Ames, A., and Alean, J. (1998). Glaciers in South America. *Studies and Reports in Hydrology*, 56:125–146.

Citterio, M., Paul, F., Ahlstrøm, A. P., Jepsen, H. F., and Weidick, A. (2009). Remote sensing of glacier change in West Greenland: accounting for the occurrence of surge-type glaciers. *Annals of Glaciology*, 50(53):70–80.

Clarke, G. K., Collins, S. G., and Thompson, D. E. (1984). Flow, thermal structure, and subglacial conditions of a surge-type glacier. *Canadian Journal of Earth Sciences*, 21(2):232–240.

Copland, L., Pope, S., Bishop, M. P., Shroder, J. F., Clendon, P., Bush, A., Kamp, U., Seong, Y. B., and Owen, L. A. (2009). Glacier velocities across the central Karakoram. *Annals of Glaciology*, 50(52):41–49.

Copland, L., Sharp, M. J., and Dowdeswell, J. A. (2003). The distribution and flow characteristics of surge-type glaciers in the Canadian High Arctic. *Annals of Glaciology*, 36:73–81.

Copland, L., Sylvestre, T., Bishop, M. P., Shroder, J. F., Seong, Y. B., Owen, L. A., Bush, A., and Kamp, U. (2011). Expanded and recently increased glacier surging in the Karakoram. *Arctic, Antarctic, and Alpine Research*, 43(4):503–516.

Dallman, W. K. (2002-2012). Geologi svalbard s250.

Das, S. B., Joughin, I., Behn, M. D., Howat, I. M., King, M. A., Lizarralde, D., and Bhatia, M. P. (2008). Fracture propagation to the base of the Greenland ice sheet during supraglacial lake drainage. *Science*, 320(5877):778–781.

Dehecq, A., Millan, R., Berthier, E., Gourmelen, N., Trouvé, E., and Vionnet, V. (2016). Elevation changes inferred from tandem-x data over the mont-blanc area: Impact of the x-band interferometric bias. *IEEE Journal of Selected Topics in Applied Earth Observations and Remote Sensing*, 9(8):3870–3882.

Dolgoushin, L. and Osipova, G. (1975). Glacier surges and the problem of their forecasting. *IAHS Publ*, 104:292–304.

Domingues, C. M., Church, J. A., White, N. J., Gleckler, P. J., Wijffels, S. E., Barker, P. M., and Dunn, J. R. (2008). Improved estimates of upper-ocean warming and multi-decadal sea-level rise. *Nature*, 453(7198):1090.

Dowdeswell, J., Drewry, D., Liestøl, O., and Orheim, O. (1984a). Radio echo-sounding of Spitsbergen glaciers: problems in the interpretation of layer and bottom returns. *Journal of Glaciology*, 30(104):16–21.

Dowdeswell, J., Hodgkins, R., Nuttall, A.-M., Hagen, J., and Hamilton, G. (1995). Mass balance change as a control on the frequency and occurrence of glacier surges in Svalbard, Norwegian High Arctic. *Geophysical Research Letters*, 22(21):2909–2912.

Dowdeswell, J. A., Drewry, D. J., Liestøl, O., and Orheim, O. (1984b). *Airborne radio echo sounding of sub-polar glaciers in Spitsbergen.*

Dowdeswell, J. A., Hamilton, G. S., and Hagen, J. O. (1991). The duration of the active phase on surge-type glaciers: contrasts between Svalbard and other regions. *Journal of Glaciology*, 37(127):388–400.

Dowdeswell, J. A. and Ottesen, D. (2016). Eskers formed at the beds of modern surge-type tidewater glaciers in Spitsbergen. *Geological Society, London, Memoirs*, 46(1):83–84.

Dowdeswell, J. A. and Williams, M. (1997). Surge-type glaciers in the Russian High Arctic identified from digital satellite imagery. *Journal of Glaciology*, 43(145):489–494.

Dunse, T., Schellenberger, T., Hagen, J., Kääb, A., Schuler, T. V., and Reijmer, C. (2015). Glacier-surge mechanisms promoted by a hydro-thermodynamic feedback to summer melt. *The Cryosphere*, 9(1):197–215.

Dyurgerov, M. B., Meier, M. F., et al. (2005). *Glaciers and the changing Earth system: a 2004 snapshot*, volume 58. Institute of Arctic and Alpine Research, University of Colorado Boulder.

Eisen, O., Harrison, W. D., Raymond, C. F., Echelmeyer, K. A., Bender, G. A., and Gorda, J. L. (2005). Variegated glacier, alaska, usa: a century of surges. *Journal of Glaciology*, 51(174):399–406.

Espizúa, L. E. (1986). Fluctuations of the rio del plomo glaciers. *Geografiska Annaler: Series A, Physical Geography*, 68(4):317–327.

Eyles, N. (2008). Glacio-epochs and the supercontinent cycle after 3.0 ga: tectonic boundary conditions for glaciation. *Palaeogeography, Palaeoclimatology, Palaeoecology*, 258(1-2):89–129.

Fischer, A., Rott, H., and Björnsson, H. (2003). Observation of recent surges of Vatnajökull, iceland, by means of ers sar interferometry. *Annals of Glaciology*, 37:69–76.

Flink, A. E., Noormets, R., Kirchner, N., Benn, D. I., Luckman, A., and Lovell, H. (2015). The evolution of a submarine landform record following recent and multiple surges of tunabreen glacier, svalbard. *Quaternary Science Reviews*, 108:37–50.

Fountain, A. G., Jacobel, R. W., Schlichting, R., and Jansson, P. (2005). Fractures as the main pathways of water flow in temperate glaciers. *Nature*, 433(7026):618.

Fowler, A. (1986). Sub-temperate basal sliding. *Journal of Glaciology*, 32(110):3–5.

Fowler, A., Murray, T., and Ng, F. (2001). Thermally controlled glacier surging. *Journal of Glaciology*, 47(159):527–538.

Frappé, T.-P. and Clarke, G. K. (2007). Slow surge of Trapridge Glacier, Yukon Territory, canada. *Journal of Geophysical Research: Earth Surface*, 112(F3).

Gardner, A. S., Moholdt, G., Wouters, B., Wolken, G. J., Burgess, D. O., Sharp, M. J., Cogley, J. G., Braun, C., and Labine, C. (2011). Sharply increased mass loss from glaciers and ice caps in the Canadian Arctic Archipelago. *Nature*, 473(7347):357.

Girod, L., Nuth, C., Kääb, A., McNabb, R., and Galland, O. (2017). Mmaster: improved aster dems for elevation change monitoring. *Remote Sensing*, 9(7):704.

Glen, J. W. (1955). The creep of polycrystalline ice. *Proceedings of the Royal Society of London. Series A. Mathematical and Physical Sciences*, 228(1175):519–538.

Grant, K. L., Stokes, C. R., and Evans, I. S. (2009). Identification and characteristics of surge-type glaciers on Novaya Zemlya, Russian Arctic. *Journal of Glaciology*, 55(194):960–972.

Gripp, K. (1929). Glaciologische und geologische ergebnisse der hamburgischen spitzbergen-expedition 1927: mit 32 tafeln und 39 figuren im text. *Abhandlungen aus dem Gebiete der Naturwissenschaften*, 22(3/4):145–249.

Gulley, J. and Benn, D. (2007). Structural control of englacial drainage systems in himalayan debris-covered glaciers. *Journal of Glaciology*, 53(182):399–412.

Gulley, J., Benn, D., Müller, D., and Luckman, A. (2009). A cut-and-closure origin for englacial conduits in uncrevassed regions of polythermal glaciers. *Journal of Glaciology*, 55(189):66–80.

Hamilton, G. S. and Dowdeswell, J. A. (1996). Controls on glacier surging in Svalbard. *Journal of Glaciology*, 42(140):157–168.

Harland, W. B. (1997). Svalbard. *Geological Society, London, Memoirs*, 17(1):3–15.

Hewitt, K. (1969). Glacier surges in the Karakoram Himalaya (central Asia). *Canadian Journal of Earth Sciences*, 6(4):1009–1018.

Hewitt, K. (1998). Recent glacier surges in the karakoram himalaya, south central asia. *Eos*, 78:46.

Hewitt, K. (2007). Tributary glacier surges: an exceptional concentration at Panmah Glacier, Karakoram Himalaya. *Journal of Glaciology*, 53(181):181–188.

Hisdal, V. (1985). *Geography of Svalbard*. Norsk Polarinst.

Hodgkins, R. (1997). Glacier hydrology in Svalbard, Norwegian high arctic. *Quaternary Science Reviews*, 16(9):957–973.

Hodson, T., Gooch, D. L., and Stuart, G. W. (1997). Structures within the surge front at bakaninbreen, svalbard, using ground-penetrating radar. *Annals of Glaciology*, 24:122–129.

Hoinkes, H. C. (1969). Surges of the Vernagtferner in the Ötztal Alps since 1599. *Canadian Journal of Earth Sciences*, 6(4):853–861.

Howat, I. M., Box, J. E., Ahn, Y., Herrington, A., and McFADDEN, E. M. (2010). Seasonal variability in the dynamics of marine-terminating outlet glaciers in Greenland. *Journal of Glaciology*, 56(198):601–613.

Iken, A. and Bindschadler, R. A. (1986). Combined measurements of subglacial water pressure and surface velocity of Findelengletscher, Switzerland: conclusions about drainage system and sliding mechanism. *Journal of Glaciology*, 32(110):101–119.

Jafarov, E. E., Marchenko, S. S., and Romanovsky, V. (2012). Numerical modeling of permafrost dynamics in Alaska using a high spatial resolution dataset. *The Cryosphere*, 6(3):613–624.

Jiskoot, H., Boyle, P., and Murray, T. (1998). The incidence of glacier surging in svalbard: evidence from multivariate statistics. *Computers & Geosciences*, 24(4):387–399.

Jiskoot, H., Jiskoot, H., Luckman, A., and Murray, T. (2001). Controls on surging in east greenland derived from a new glacier inventory. In *AGU Fall Meeting Abstracts*.

Jiskoot, H., Murray, T., and Luckman, A. (2003). Surge potential and drainage-basin characteristics in East Greenland. *Annals of Glaciology*, 36:142–148.

Joughin, I., Howat, I. M., Fahnestock, M., Smith, B., Krabill, W., Alley, R. B., Stern, H., and Truffer, M. (2008). Continued evolution of Jakobshavn Isbrae following its rapid speedup. *Journal of Geophysical Research: Earth Surface*, 113(F4).

Kääb, A. (2005). *Remote sensing of mountain glaciers and permafrost creep*, volume 48. Geograph. Inst. d. Univ.

Kääb, A., Leinss, S., Gilbert, A., Bühler, Y., Gascoin, S., Evans, S. G., Bartelt, P., Berthier, E., Brun, F., Chao, W.-A., et al. (2018). Massive collapse of two glaciers in western Tibet in 2016 after surge-like instability. *Nature Geoscience*, 11(2):114.

Kamb, B. (1970). Sliding motion of glaciers: theory and observation. *Reviews of Geophysics*, 8(4):673–728.

Kamb, B. and LaChapelle, E. (1964). Direct observation of the mechanism of glacier sliding over bedrock. *Journal of Glaciology*, 5(38):159–172.

Kamb, B., Raymond, C., Harrison, W., Engelhardt, H., Echelmeyer, K., Humphrey, N., Brugman, M., and Pfeffer, T. (1985). Glacier surge mechanism: 1982-1983 surge of Variegated Glacier, Alaska. *Science*, 227(4686):469–479.

King, O., Hambrey, M. J., Irvine-Fynn, T. D., and Holt, T. O. (2016). The structural, geometric and volumetric changes of a polythermal Arctic glacier during a surge cycle: Comfortlessbreen, Svalbard. *Earth Surface Processes and Landforms*, 41(2):162–177.

Kotliakov, V. M. (1996). *Variations of snow and ice in the past and at present on a global and regional scale*. UNESCO.

Kotlyakov, V., Osipova, G., and Tsvetkov, D. (2008). Monitoring surging glaciers of the Pamirs, central Asia, from space. *Annals of Glaciology*, 48:125–134.

Kotlyakov, V. M., Rototaeva, O., and Nosenko, G. (2004). The september 2002 Kolka glacier catastrophe in North Ossetia, Russian Federation: evidence and analysis. *Mountain Research and Development*, 24(1):78–84.

Kuglin, C. and Hines, D. (1975). The phase correlation image alignment method. inproceedings of the ieee international conference on cybernetics andsociety.

Lefauconnier, B. and Hagen, J. O. (1991). *Surging and calving glaciers in eastern Svalbard*.

Leprince, S., Barbot, S., Ayoub, F., and Avouac, J.-P. (2007). Automatic and precise orthorectification, coregistration, and subpixel correlation of satellite images, application to ground deformation measurements. *IEEE Transactions on Geoscience and Remote Sensing*, 45(6):1529–1558.

Liestøl, O. (1969). Glacier surges in west Spitsbergen. *Canadian Journal of Earth Sciences*, 6(4):895–897.

Lillesand, T., Kiefer, R. W., and Chipman, J. (2014). *Remote sensing and image interpretation*. John Wiley & Sons.

Lliboutry, L. (1968). General theory of subglacial cavitation and sliding of temperate glaciers. *Journal of Glaciology*, 7(49):21–58.

Lliboutry, L. (1987). Realistic, yet simple bottom boundary conditions for glaciers and ice sheets. *Journal of Geophysical Research: Solid Earth*, 92(B9):9101–9109.

Luckman, A., Benn, D. I., Cottier, F., Bevan, S., Nilsen, F., and Inall, M. (2015). Calving rates at tidewater glaciers vary strongly with ocean temperature. *Nature communications*, 6:8566.

Mansell, D., Luckman, A., and Murray, T. (2012). Dynamics of tidewater surge-type glaciers in northwest Svalbard. *Journal of Glaciology*, 58(207):110–118.

Martín Español, A., Navarro Valero, F. J., Otero García, J., Lapazaran Izargain, J. J., and Blaszczyk, M. (2015). Estimate of the total volume of svalbard glaciers, and their potential contribution to sea-level rise, using new regionally based scaling relationships. *Journal of Glaciology*, 61(225):29–41.

McNabb, R. and Hock, R. (2014). Alaska tidewater glacier terminus positions, 1948–2012. *Journal of Geophysical Research: Earth Surface*, 119(2):153–167.

Meier, M. F. and Post, A. (1969). What are glacier surges? *Canadian Journal of Earth Sciences*, 6(4):807–817.

Melvold, K. and Hagen, J. O. (1998). Evolution of a surge-type glacier in its quiescent phase: Kongsvegen, Spitsbergen, 1964–95. *Journal of Glaciology*, 44(147):394–404.

Moon, T. and Joughin, I. (2008). Retreat and advance of Greenland tidewater glaciers from 1992 to 2007. *J. Geophys. Res*, 113(345):F02022.

Mørk, A., Dallmann, W., Dypvik, H., Johannessen, E., Larssen, G., Nagy, J., Nøttvedt, A., Olaussen, S., Pchelina, T., and Worsley, D. (1999). Mesozoic lithostratigraphy. *Lithostratigraphic lexicon of Svalbard. Upper Palaeozoic to Quaternary bedrock. Review and recommendations for nomenclature use*, pages 127–214.

Murray, T., James, T. D., Macheret, Y., Lavrentiev, I., Glazovsky, A., and Sykes, H. (2012). Geometric changes in a tidewater glacier in Svalbard during its surge cycle. *Arctic, Antarctic, and Alpine research*, 44(3):359–367.

Murray, T., Strozzi, T., Luckman, A., Jiskoot, H., and Christakos, P. (2003). Is there a single surge mechanism? Contrasts in dynamics between glacier surges in Svalbard and other regions. *Journal of Geophysical Research: Solid Earth*, 108(B5).

Murray, T., Stuart, G. W., Miller, P. J., Woodward, J., Smith, A. M., Porter, P. R., and Jiskoot, H. (2000). Glacier surge propagation by thermal evolution at the bed. *Journal of Geophysical Research: Solid Earth*, 105(B6):13491–13507.

Nolan, M. (2003). The "galloping glacier" trots: Decadal-scale speed oscillations within the quiescent phase. *Annals of Glaciology*, 36:7–13.

Norwegian Polar Institute (2014). Terrengmodell Svalbard (S0 Terrengmodell).

Nuth, C., Gilbert, A., Köhler, A., McNabb, R., Schellenberger, T., Sevestre, H., Weidle, C., Girod, L., Luckman, A., and Kääb, A. (2019). Dynamic vulnerability revealed in the collapse of an Arctic tidewater glacier. *Scientific reports*, 9.

Nuth, C. and Kääb, A. (2011). Co-registration and bias corrections of satellite elevation data sets for quantifying glacier thickness change. *The Cryosphere*, 5(1):271–290.

Nuth, C., Moholdt, G., Kohler, J., Hagen, J. O., and Kääb, A. (2010). Svalbard glacier elevation changes and contribution to sea level rise. *Journal of Geophysical Research: Earth Surface*, 115(F1).

Nye, J. F. (1957). The distribution of stress and velocity in glaciers and ice-sheets. *Proceedings of the Royal Society of London. Series A. Mathematical and Physical Sciences*, 239(1216):113–133.

Ottesen, D., Dowdeswell, J., Bjarnadottir, L., and Bellec, V. (2017a). The Negribreen glacier submarine surge system, eastern Svalbard. In *EGU General Assembly Conference Abstracts*, volume 19, page 7648.

Ottesen, D., Dowdeswell, J. A., Bellec, V., and Bjarnadóttir, L. (2017b). The geomorphic imprint of glacier surges into open-marine waters: examples from eastern Svalbard. *Marine Geology*, 392:1–29.

Phillips, T., Rajaram, H., and Steffen, K. (2010). Cryo-hydrologic warming: A potential mechanism for rapid thermal response of ice sheets. *Geophysical Research Letters*, 37(20).

Porter, C., Morin, P., Howat, I., Noh, M.-J., Bates, B., Peterman, K., Keesey, S., Schlenk, M., Gardiner, J., Tomko, K., Willis, M., Kelleher, C., Cloutier, M., Husby, E., Foga, S., Nakamura, H., Platson, M., Wethington, Michael, J., Williamson, C., Bauer, Gregory; Enos, J., Arnold, G., Kramer, W., Becker, P., Doshi, A., D'Souza, C., Cummens, P., Laurier, F., and Bojesen, M. (Accessed December 2018). "arcticdem", v1. *Harvard Dataverse. doi:https://doi.org/10.7910/DVN/OHHUKH.[accessed December 2018].*

Post, A. (1969). Distribution of surging glaciers in western North America. *Journal of Glaciology*, 8(53):229–240.

Rahmstorf, S., Foster, G., and Cazenave, A. (2012). Comparing climate projections to observations up to 2011. *Environmental Research Letters*, 7(4):044035.

Raymond, C. (1996). Shear margins in glaciers and ice sheets. *Journal of Glaciology*, 42(140):90–102.

Raymond, C. F. (1987). How do glaciers surge? A review. *Journal of Geophysical Research: Solid Earth*, 92(B9):9121–9134.

Rignot, E., Box, J., Burgess, E., and Hanna, E. (2008). Mass balance of the Greenland ice sheet from 1958 to 2007. *Geophysical Research Letters*, 35(20).

Robin, G. d. Q. (1955). Ice movement and temperature distribution in glaciers and ice sheets. *Journal of Glaciology*, 2(18):523–532.

Röthlisberger, H. (1969). Evidence for an ancient glacier surge in the Swiss Alps. *Canadian Journal of Earth Sciences*, 6(4):863–865.

Röthlisberger, H. (1972). Water pressure in intra-and subglacial channels. *Journal of Glaciology*, 11(62):177–203.

Sanli, F. B. and Abdikan, S. (2006). copmaring a stereoscopic dem with an interformetric dem using the same radarsat data pair. In *ISPRS Commission VII Mid-term Symposium" Remote Sensing: From Pixels to Processes.*

Scambos, T., Fahnestock, M., Moon, T., Gardner, A., and Klinger, M. (Accessed December 2018). Global land ice velocity extraction from landsat 8 (go-live), version 1.[subsets: p209_r004, p210_r004, p211_r004, p212_r004, p213_r003, p213_r004, p214_r003, p214_r004, p215_r003, p216_r003, p217_r003, p218_r003, p219_r003]. *Boulder, Colorado USA. NSIDC: National Snow and Ice Data Center. doi: https://doi.org/10.7265/N5ZP442B.[accessed December 2018].*

Scharroo, R. and Visser, P. (1998). Precise orbit determination and gravity field improvement for the ERS satellites. *Journal of Geophysical Research: Oceans*, 103(C4):8113–8127.

Schellenberger, T., Dunse, T., Kääb, A., Kohler, J., and Reijmer, C. (2014). Surface speed and frontal ablation of Kronebreen and Kongsbreen, NW-Svalbard, from sar offset tracking. *The Cryosphere Discussions*, 8:6193–6233.

Schild, K. M. and Hamilton, G. S. (2013). Seasonal variations of outlet glacier terminus position in Greenland. *Journal of Glaciology*, 59(216):759–770.

Sevestre, H., Benn, D. I., Hulton, N. R., and Bælum, K. (2015). Thermal structure of Svalbard glaciers and implications for thermal switch models of glacier surging. *Journal of Geophysical Research: Earth Surface*, 120(10):2220–2236.

Sevestre, H., Benn, D. I., Luckman, A., Nuth, C., Kohler, J., Lindbäck, K., and Pettersson, R. (2018). Tidewater glacier surges initiated at the terminus. *Journal of Geophysical Research: Earth Surface*, 123(5):1035–1051.

Sharp, M. (1988). Surging glaciers: behaviour and mechanisms. *Progress in Physical Geography*, 12(3):349–370.

Stenborg, T. (1969). Studies of the internal drainage of glaciers. *Geografiska Annaler: Series A, Physical Geography*, 51(1-2):13–41.

Stevens, L. A., Behn, M. D., McGuire, J. J., Das, S. B., Joughin, I., Herring, T., Shean, D. E., and King, M. A. (2015). Greenland supraglacial lake drainages triggered by hydrologically induced basal slip. *Nature*, 522(7554):73.

Stroeve, J. C., Serreze, M. C., Holland, M. M., Kay, J. E., Malanik, J., and Barrett, A. P. (2012). The Arctic's rapidly shrinking sea ice cover: A research synthesis. *Climatic Change*, 110(3-4):1005–1027.

Subcommittee, P. (1988). Glossary of permafrost and related ground-ice terms. *Associate Committee on Geotechnical Research, National Research Council of Canada, Ottawa*, 156.

Sugden, D. E. and John, B. S. (1976). *Glaciers and landscape*. E. Arnold.

Sund, M., Eiken, T., Hagen, J. O., and Kääb, A. (2009). Svalbard surge dynamics derived from geometric changes. *Annals of Glaciology*, 50(52):50–60.

Sund, M., Eiken, T., and Rolstad Denby, C. (2011). Velocity structure, front position changes and calving of the tidewater glacier Kronebreen, Svalbard. *The Cryosphere Discussions*, 5(1):41–73.

Thorarinsson, S. (1969). Glacier surges in iceland, with special reference to the surges of Brúarjökull. *Canadian Journal of Earth Sciences*, 6(4):875–882.

Tivy, A., Howell, S. E., Alt, B., McCourt, S., Chagnon, R., Crocker, G., Carrieres, T., and Yackel, J. J. (2011). Trends and variability in summer sea ice cover in the Canadian Arctic based on the Canadian Ice Service digital archive, 1960–2008 and 1968–2008. *Journal of Geophysical Research: Oceans*, 116(C3).

Toutin, T. (2008). Aster dems for geomatic and geoscientific applications: a review. *International Journal of Remote Sensing*, 29(7):1855–1875.

Van der Veen, C. J. (2013). *Fundamentals of glacier dynamics*. CRC Press.

Vaughan, D. G., Comiso, J. C., Allison, I., Carrasco, J., Kaser, G., Kwok, R., Mote, P., Murray, T., Paul, F., Ren, J., et al. (2013). Observations: Cryosphere. *Climate change*, 2103:317–382.

von Heuglin, T. (1872). *Reisen nach dem Nordpolarmeer in den Jahren 1870 und 1871*. Ripol Classic.

Waller, R. (2001). The influence of basal processes on the dynamic behaviour of cold-based glaciers. *Quaternary International*, 86(1):117–128.

Wassiliew, A. (1925). *Spitsberg III. Feuille du Sud (topographic map 1:200 000). In Missions scientifiques pour la mesure d'un arc de méridien au Spitsberg.*

Weber, J. E. (2000). Non-temperate glacier flow over wavy sloping ground. *Journal of Glaciology*, 46(154):453–458.

Weertman, J. (1964). The theory of glacier sliding. *Journal of Glaciology*, 5(39):287–303.

Wenjing, Z. (1992). Identification of glaciers with surge characteristics on the Tibetan Plateau. *Annals of Glaciology*, 16:168–172.

Willis, I. C. (1995). Intra-annual variations in glacier motion: a review. *Progress in Physical Geography*, 19(1):61–106.

Yagüe-Martínez, N., Prats-Iraola, P., Gonzalez, F. R., Brcic, R., Shau, R., Geudtner, D., Eineder, M., and Bamler, R. (2016). Interferometric processing of Sentinel-1 TOPS data. *IEEE Transactions on Geoscience and Remote Sensing*, 54(4):2220–2234.

Yde, J. C. and Knudsen, N. T. (2007). 20th-century glacier fluctuations on Disko Island (qeqertarsuaq), greenland. *Annals of Glaciology*, 46:209–214.